*Korean J. Chem. Eng.*, 35(7), 1389-1408 (2018)
DOI: 10.1007/s11814-018-0089-6

pISSN: 0256-1115
eISSN: 1975-7220

**INVITED REVIEW PAPER**

# A review on metal nitrides/oxynitrides as an emerging supercapacitor electrode beyond oxide

**Subrata Ghosh*, Sang Mun Jeong*,†, and Shyamal Rao Polaki****

*Green Energy Lab., Department of Chemical Engineering, Chungbuk National University, 1 Chungdae-ro, Seowon-gu, Cheongju, Chungbuk 28644, Korea
**Surface and Nanoscience Division, Materials Science Group, Indira Gandhi Centre for Atomic Research, Kalpakkam 603102, India

(*Received 18 March 2018 • accepted 27 May 2018*)

**Abstract**−Electrode materials design is the most significant aspect in constructing a supercapacitor device. The evolution of metal nitrides/oxynitrides as supercapacitor electrode is strikingly noticeable today besides prevailing carbon or 2D materials, metal oxides/hydroxides and conducting polymers electrode materials. The theoretically estimated specific capacitance of a nitride-based supercapacitor is 1,560 F $g^{-1}$. These nanostructures exhibit an excellent capacitive behavior with a specific capacitance of 15-951.3 mF $cm^{-2}$ or 82-990 F $g^{-1}$, high energy density (16.5-162 Wh $Kg^{-1}$) and power density (7.3-54,000 W $Kg^{-1}$). On this account, supercapacitor performance of metal nitrides/oxynitrides is reviewed exclusively. The major focus of the present review is directed towards state-of-art progress in supercapacitor performance of nitrides/oxynitrides, underlying charge-storage mechanism, important outcomes and their limitations. Finally, we conclude with challenges and prospects of metal nitrides/oxynitrides for supercapacitor electrodes.

Keywords: Supercapacitor, Energy Storage Materials, Metal Nitrides, Metal Oxynitrides, Pseudocapacitance

## INTRODUCTION

Increasing impetus in renewable energy sources and the identification of the prosperity of green energy development of sustainable energy storage device has gained much attention. The electrochemical supercapacitor, a promising energy storage device, is expecting an escalation in energy research to meet the energy challenges in the twenty-first century. In-particular, supercapacitors have foremost advantages like moderate energy density, high power density, fast charge-discharge (order of 10 sec), and prolonged cycle-life (around $10^5$ cycles). They even can bridge the gap between conventional high-energy batteries and high-power capacitors (Fig. 1(a)) [1]. Hence, a rapid growth in worldwide research interest for realizing the supercapacitor devices in day-to-day applications includes hybrid electric vehicle, emergency doors of aircraft, memory back-up systems as well as portable electronic devices such as digital telecommunication systems, cellular phones, uninterruptable power supplies, bio-medical devices and various micro-devices [2-4].

Nevertheless, the bottleneck of the supercapacitor is low energy density compared to conventional batteries and fuel cells (Fig. 1(b)). To overcome the problem, designing suitable electroactive materials and selecting a suitable electrolyte combination are crucial in

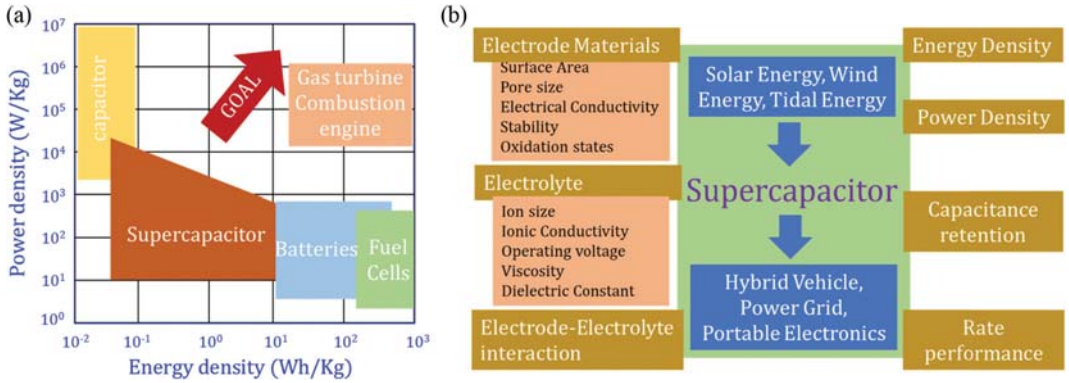


**Fig. 1. (a) Ragone plot of energy storage devices, (b) schematic of key parameters, source of energy and role of supercapacitor.**

†To whom correspondence should be addressed.
E-mail: smjeong@chungbuk.ac.kr
Copyright by The Korean Institute of Chemical Engineers.

boosting the energy harvesting. The electrolyte may be aqueous or organic, where the former one enables the device to operate within a thermodynamic potential window of 1.23 V, while maximum of a 4 V potential window can be achieved using an organic electrolyte. However, the organic electrolyte is toxic, moisture-sensitive and costly compared to its aqueous counterpart. Additionally, the electronic/ionic mobility and conductivity are lower for the organic electrolyte [5]. Therefore, designing an asymmetric supercapacitor has been found to be a potential alternative. On the other hand, constructing the high-performance electrode materials is a crucial challenge in realizing the desired goal of enhancing energy density without sacrificing their power density and cycle-life. Herein, the present review concentrates on the supercapacitive properties of electrode materials.

Supercapacitors are basically categorized into two classes on the basis of their charge storage mechanism: electric double layer capacitors and pseudocapacitors. The formation of an electric double layer at the electrode/electrolyte interface is responsible for the charge storage in double layer capacitance and hence specific capacitance. Carbon-based materials primarily fall into this category due to their high surface area, electronic conductivity, stability and so on [6-10]. The idea behind the charge storage of a pseudocapacitor is the chain of fast reversible redox kinetics. The state-of-art pseudocapacitor materials are transition metal oxides/hydroxides or conducting polymers [11,12]. Eventually, these materials can store a charge of the order of ten to hundred times higher than carbon-based double layer capacitors [12,13]. Hence, designing the carbon and metal oxides/hydroxides hybrid structure is the subject of intense research [14-18].

In spite of continuous progress in supercapacitor performance, metal oxides suffer from poor stability and electrical conductivity. Hence, there is an urgent need to exploit alternative electrode materials for pseudocapacitors. In view of this, metal nitrides have received an excellent opportunity as a promising substitute for the oxides. In particular, oxygen-deficient metal oxides have shown enhanced supercapacitor performance due to their improved electrical conductivity and increased pseudo-capacitance [19]. On the other hand, nitrogen doping in metal oxides or conversion of an oxide to a nitride provides an enhanced capacitance due to the inclusion of electron donor features as well as increases the overpotential of both hydrogen and oxygen evolution [20]. Hence, nitrogen substitution by replacing oxides/hydroxides completely can result in prominent electrochemical capacitive properties [21]. Additionally, metal nitrides possess excellent physico-chemical features, such as intrinsic electrical conductivity ($\approx 10^6\ \Omega^{-1}m^{-1}$), corrosion resistance to chemical attack, excellent electrochemical stability, catalytic activity, and faster charge-discharge ability. For example, the electrical conductivity of titanium nitride (TiN) is $4.5\times10^6$ S $m^{-1}$, whereas electrical conductivity of $TiO_2$ is $10^{-8}$ S $m^{-1}$ [22]. Such a huge difference in electrical conductivity and deficiencies of metal oxides has certainly motivated tremendous research attention on metal nitrides-based supercapacitors [23-26]. However, all metal nitrides cannot be used as electrodes, owing to their poor physical property [27]. For example, tantalum nitride ($Ta_3N_4$) as electrode material does not show promising capacitive properties due to poor electrical conductivity [27]. Therefore, it is of interest to review the metal nitrides for supercapacitor aspects considering the continuous energy demand.

The charge storage performance of metal nitrides is based on the interactions of surface oxide/oxynitride phase or surface redox reaction and double-layer mechanism. Not only the electrode material, but also the type of electrolyte plays a significant role in the charge storage properties [28]. The morphology and structures also highly influence the capacitive properties of the materials. Diverse morphologies of metal nitrides have been explored, for example, those in nanopowder, thin film, zero to three-dimensional structures (nanowire, nanotube, nanowalls, nanobelt, core-shell structure). To prepare those architectures, various techniques including chemical vapor deposition, hydrothermal method, chemical bath deposition technique, and sputtering have been employed in the existing studies.

This review comprises three main categories along with conclusion and challenges. In the first part, we discuss the supercapacitive properties of metal nitrides compared to metal oxide counterpart. The second part is based on the electrochemical properties of metal oxynitrides as supercapacitor electrode. Considering the advantages of two-dissimilar electrodes towards enhancing energy density, a discussion on metal nitride/oxynitride-based asymmetric supercapacitor is provided in third part. The critical aspects, key parameters, advantages and loopholes of the obtained electrode materials as well as their capacitive properties are discussed in the following sections. Finally, the conclusion includes a summary and future challenges for the supercapacitive performance of metal nitrides/oxy-nitrides based materials.

## NITRIDES AND THEIR SUPERCAPACITOR PERFORMANCES

A variety of metal nitrides have been employed as supercapacitor electrodes. These include, molybdenum nitride (MoN, $Mo_2N$), titanium nitride (TiN), vanadium nitride (VN), niobium nitride (NbN, $Nb_4N_5$), ruthenium nitride (RuN), chromium nitride (CrN), cobalt nitride (CoN), lanthanum nitride (LaN), nickel nitride ($Ni_3N$), gallium nitride (GaN), iron nitride ($Fe_2N$) and tungsten nitride (WN, $W_2N$). They not only serve as electrode but also as a mechanical backbone to other nanoarchitectures for use in supercapacitor application. The general strategy to prepare metal nitrides is either via metal oxide preparation and followed by nitridation or vapor deposition (chemical or physical). Fig. 2 illustrates the widely adopted synthesis methods for the metal nitride preparation. The supercapacitor performance of metal nitride-based material is summarized in Table 1.

### 1. Molybdenum Nitride

Molybdenum nitride is a promising material by virtue of its lower leakage current in alkaline aqueous medium, easy fabrication and high conductivity of 0.206 S $m^{-1}$. Another key factor is the wettability of molybdenum nitride. Eventually, MoN/$Mo_2N$ have emerged as the first materials in nitride family for supercapacitor electrodes [23]. A significant reduction in contact angle from $55.2^0$ to $24.3^0$ as $MoO_3$ transformed MoN has been reported, which in turn enhanced linear capacitance from 7.6 to 13.7 mF $cm^{-1}$ [90]. Around 200 times enhancement in capacitance was obtained

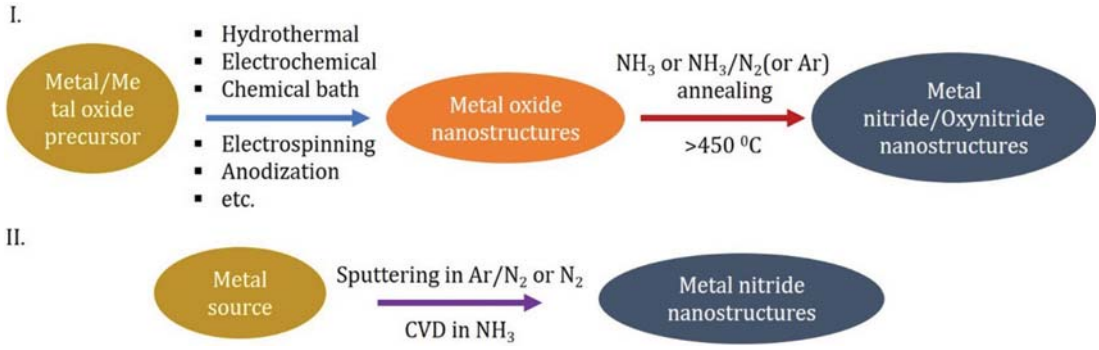


**Fig. 2. Schematic of general strategies to synthesize the metal nitride/oxynitride nanostructure.**

**Table 1. Supercapacitance performance of metal nitride-based electrode (Highest sp. Capacitance of the materials are listed from the cited literature)**

| Materials | Capacitance | Stability, cycle number | Electrolyte | Energy density | Power density | Ref. |
|---|---|---|---|---|---|---|
| $\gamma$-$Mo_2N$ | 380 F $g^{-1}$ | | 0.1 M $H_2SO_4$ | | | [28] |
| $Mo_2N$ nanobelt | 160 F $g^{-1}$ | 91%, 1000 | 1 M $H_2SO_4$ | | | [29] |
| Hunk-like $Mo_2N$<br>$Mo_2N$//AC | 171 F $g^{-1}$<br>46.8 F $g^{-1}$ | 100%, 10000 | 1 M $H_2SO_4$ | 16.5 Whkg$^{-1}$ | 8000 W $kg^{-1}$ | [30] |
| $\gamma$-$Mo_2N$/$Co_3Mo_3N$ | 109.9 F $g^{-1}$ | | 0.1 M HCL | | | [31] |
| Mesoporous $Mo_3N_2$ NW | 220 F $g^{-1}$ | | 1 M KOH | | | [32] |
| $Mo_2N$//rGO | 46.8 F $g^{-1}$ | 100%, 10000 | 1 M $H_2SO_4$ | | | [30] |
| TiN NTA<br>TiN nanopore arrays | 11.8 mF/$cm^2$<br>99.7 mF/$cm^2$ | <br>98.5%, 100 | 1 M $H_2SO_4$<br>1 M $H_2SO_4$ | 35.9 mWs $cm^{-2}$<br>or 900 mWs $cm^{-3}$ | 8.15 mW $cm^{-2}$<br>or 204 mW $cm^{-3}$ | [22] |
| Corn-like TiN (symmetric) | 20.7 F/$cm^3$ | 95%, 20000 | 1 M $LiClO_4$ | 1.5 mWh $cm^{-3}$ | 150 W $cm^{-3}$ | [33] |
| Mesoporous TiN spheres | 144 F $g^{-1}$ in 2E | | 1 M $LiPF_6$ | 45.0 Whkg$^{-1}$ | 150 W $kg^{-1}$ | [34] |
| Porous TiN on CNT, micro-SC | 18.3 mF $cm^{-2}$ | 90%, 20000 | 0.5 M $K_2SO_4$ | | | [35] |
| TiN on CNT | 81 mF $cm^{-2}$ | | 1 M KOH | | | [36] |
| TiN/rGO | 415 F $g^{-1}$ | 93%, 10000 | 1 M $Na_2SO_4$ | | | [37] |
| $MnO_2$-TiN NTA | 853.3 F/g<br>4.01 Fcm$^{-3}$ SSC | 91.7%, 1000 | 1 M KOH | 1.81 mWh $cm^{-3}$ | 32.8 mW $cm^{-3}$ | [38] |
| TiN-$Li_4Ti_5O_{12}$ NTA | 143.83 F $g^{-1}$<br>40.45 F $g^{-1}$ for SSC | 82.4%, 1000 | 2 M LiOH | 32.36 Wh $kg^{-1}$ | 0.6 kW $kg^{-1}$ | [39] |
| TiN@$Ni(OH)_2$ core-shell NWA | 2680 F $g^{-1}$ | ~20%, 250 | 2 M KOH | | | [40] |
| $Ni_xCo_{2x}(OH)_{6x}$ coated TiN NTA | 2543 F $g^{-1}$ | 93.75%, 5000 | KOH+KCl | | | [41] |
| Core (TiN NW)-Carbon(shell) | 124.5 F $g^{-1}$ | 95%, 15000 | 1 M KOH | | | [42] |
| PANI/TiN NTA | 242 mF $cm^{-2}$ | 83%, 3000 | 1 M HCl | | | [43] |
| PANI/TiN NWA | 1064 F $g^{-1}$ | 95%, 200 | 1 M $H_2SO_4$ | | | [44] |
| Polypyrrole/TiN | 1265 F $g^{-1}$ | 72.6%, 2000 | 1 M $H_2SO_4$ | 160-39 Wh $kg^{-1}$ | 90-1350 W $kg^{-1}$ | [45] |
| PANI/carbon/TiN | 1093 F $g^{-1}$ | 98%, 2000 | 1 M $H_2SO_4$ | | | [46] |
| Polypyrrole/TiN/PANI NT | 1077.4 F $g^{-1}$<br>288.4 F $g^{-1}$ device | 78%, 200 | 1 M $H_2SO_4$ | 129.8 Wh $kg^{-1}$ | 0.9 kW $kg^{-1}$ | [47] |
| $PM_{O12}$/PANI/TIN NWA | 469 F $g^{-1}$<br>69 F $g^{-1}$ SSC | 65%, 1000 | 1 M $H_2SO_4$ | 21.6 Wh $kg^{-1}$<br>0.54 Wh $cm^{-3}$ | 375 W $kg^{-1}$<br>7.5 mW $cm^{-3}$ | [48] |
| PANI/$MnO_2$/TiN NWA | 674 F $g^{-1}$ | | | | | [49] |

**Table 1. Continued**

| Materials | Capacitance | Stability, cycle number | Electrolyte | Energy density | Power density | Ref. |
|---|---|---|---|---|---|---|
| $MoN_x$/TiN NTA | 121 mF $cm^{-2}$ | 93.8%, 1000 | 1 M LiOH | | | [50] |
| Si/TiN/$MnO_2$ taper nanorods | 81.6 mF $cm^{-2}$ | 95.7%, 5000 | 1 M $Na_2SO_4$ | | | [51] |
| TiN//TiN@$MnO_2$ | 1.1 F $cm^{-3}$ | 98.3, 5000 | LiCl-PVA | 0.55 mWh $cm^{-3}$ | 1.53 W $cm^{-3}$ | [52] |
| TiN/Porous Si | 15 F $cm^{-3}$ | 13000 | 1 M NaCl | 1.3 mWh $cm^{-3}$ | 214 W $cm^{-3}$ | [100] |
| $Fe_2N$-$Ti_2N$ core-shell | 82 F $g^{-1}$ | 99%, 20,000 | LiCl-PVA | 48.5 Wh $kg^{-1}$ | 2700 W$kg^{-1}$ | [21] |
| $Fe_2N$//TiN | 58 F $g^{-1}$ | 98%, 20000 | LiCl-PVA | 0.61 mWh $cm^{-3}$ | 52.9 mWh $cm^{-3}$ | [53] |
| VN | 234 F $g^{-1}$ | | 0.1 M KOH | | | [28] |
| Nanocrystalline VN | 413 F $g^{-1}$ | 60%, 1000 | 1 M KOH | | | [54] |
| VN nanopowder | 850 F $g^{-1}$ | | 1 M KOH | | | [55] |
| VN thin film | 422 F $g^{-1}$ | 69%, 1000 | 1 M KOH | 0.01 Wh $cm^{-3}$ | 125 W $cm^{-3}$ | [56] |
| Porous VN hollow NF | 115 F $g^{-1}$ | 54%, 1000 | 2 M KOH | | | [57] |
| Porous VN nanowires | 298.5 F $g^{-1}$ | 95.3%,10000 | LiCl-PVA | | | [58] |
| VN Nanords | 186 F $g^{-1}$ | | 1 M KOH | | | [59] |
| Mesoporous VN | 598 F $g^{-1}$ | 83%, 5000 | 6 M KOH | | | [60] |
| VN QD/N-doped CNF | 406.5 F $g^{-1}$ | 75.3%, 1000 | 6 M KOH | | | [61] |
| VN-carbon fiber | 800 F $g^{-1}$ | | 6 M KOH | | | [62] |
| VN@N-doped carbon NW | 282 mF $cm^{-2}$ | 91.8%, 12000 | 6 M KOH | 0.97 mWh $cm^{-3}$ | 2.72 W $cm^{-3}$ | [63] |
| VN nanotrees on CNT | 37.5 mF $cm^{-2}$ | 85%, 20000 | 0.5 M $Na_2SO_4$ | | | [64] |
| $Co_3O_4$//CNS@VN | 300 F $g^{-1}$ (CNS@VN) | 77.3%, 5000 | 6 M KOH | 18.8 Wh $kg^{-1}$ | 800 W $kg^{-1}$ | [65] |
| Core (VN NW)-Carbon(shell) | 46.9 F $g^{-1}$ | 88.4%, 15000 | 1 M KOH | | | [42] |
| VN/N-doped graphene | 445 F $g^{-1}$ | 98.6%, 10000 | 6 M KOH | 81.73 Wh $kg^{-1}$ | 28.82 kW $kg^{-1}$ | [66] |
| Mesoporous VN NW/NC | 282 mF $cm^{-2}$ | 91.8%, 12000 | 6 M KOH | | | [63] |
| VN/CNT | 7.9 F $cm^{-3}$ | 82%, 10000 | $H_3PO_4$/PVA | 0.54 mWh $cm^{-3}$ | 0.4 W $cm^{-3}$ | [116] |
| 3D porous VN NW-Graphene//APDC for LIC | 73 F $g^{-1}$ | 83%, 1000 | 1 M $LiPF_6$ (EC/DEC) | 162 Wh $kg^{-1}$<br>64 Wh $kg^{-1}$ | 200 W $kg^{-1}$<br>10 kW $kg^{-1}$ | [67] |
| VN//NiO | 1.85 mF $cm^{-2}$ | 10,000 | 1 M KOH | 1.0 μWh$cm^{-2}$ | 40 mW$cm^{-2}$ | [68] |
| $VO_x$ NW//VN NW | 1.35 F $cm^{-3}$ | 87.5%, 10000 | LiCl-PVA | 0.61 mWh $cm^{-3}$ | 0.85 W $cm^{-3}$ | [58] |
| $Co(OH)_2$//VN | 62.4 F $g^{-1}$ | | 2 M KOH | 22 Wh $kg^{-1}$ | 0.16 kW $kg^{-1}$ | [69] |
| CF@VN//AC | 23.28 F $g^{-1}$ | 82%, 1000 | 2 M $NaNO_3$ | 8.24 Wh $kg^{-1}$ | 400 W $kg^{-1}$ | [120] |
| VN/CF//$Ni(OH)_2$ | 188 F $g^{-1}$ | 96.4%, 10000 | 6 M KOH | 53-36 Wh $kg^{-1}$ | 2.7-54 kW $kg^{-1}$ | [62] |
| VNQD/PC//$Ni(OH)_2$ | 122.5 F $g^{-1}$ | 68.6%, 4000 | 6 M KOH | 47.2 Wh $kg^{-1}$ | 828.7 W $kg^{-1}$ | [70] |
| $MnO_2$-CNT//VN-CNT | 43 F $cm^{-3}$ | 80%, 1000 | 0.5 M $Na_2SO_4$ | 38.7 Wh $kg^{-1}$<br>19.4 mWh $cm^{-3}$ | 7.3 W $kg^{-1}$<br>3.7 mW $cm^{-3}$ | [71] |
| VTiN/C NF | 430.7 F $g^{-1}$ | 37%, 600 | 1 M KOH | | | [72] |
| (Ti,V)N | 15 mF $cm^{-2}$ | 99%, 10000 | 1 M KOH | | | [73] |
| Ni NP@Ni-Mo-N | 4.892 F $cm^{-2}$ | 80.1%, 6000 | 6 M KOH | 40.9 Wh $kg^{-1}$ | 773 W $kg^{-1}$ | [74] |
| $Nb_4N_5$ | 225.8 mF $cm^{-2}$ | 70.9%, 2000 | 1 M $H_2SO_4$ | 4.66 mWh $cm^{-3}$ | 24.56 W $cm^{-3}$ | [75] |
| NbN/NG for LIC | ~30 mAh $g^{-1}$ | 81.7%, 1000 | 1 M $LiPF_6$-EC/DMC | 122.7-98.4 Wh $kg^{-1}$ | 100-2000 W $kg^{-1}$ | [119] |
| CoN//AC<br>CrN//AC | 37 F $g^{-1}$<br>75 F $g^{-1}$ | 27%, 100<br>100%, 120 | 1 M $LiPF_6$ (EC/DEC) | 44 Wh $kg^{-1}$<br>30 Wh $kg^{-1}$ | | [76] |

**Table 1. Continued**

| Materials | Capacitance | Stability, cycle number | Electrolyte | Energy density | Power density | Ref. |
|---|---|---|---|---|---|---|
| $Fe_2N$-activated carbon | 507 F $g^{-1}$ | | 6 M KOH | | | [77] |
| $Fe_2N$-OMC | 547 F $g^{-1}$ | 76%, 1000 | 6 M KOH | | | [78] |
| GaN NW | 227 mF $cm^{-2}$ | 98%, 10000 | 1 M $H_2SO_4$ | 0.30 mW h $cm^{-3}$ | 1000 mW $cm^{-3}$ | [79] |
| RuN | 37 $g^{-1}$ | | 1 M $LiPF_6$ | | | [80] |
| LaN | 951.3 F $cm^{-3}$ | 99%, 5000 | $Na_2SO_4$ | ~$10^2$ Wh $L^{-1}$ | ~$3\times10^4$ W $L^{-1}$ | [81] |
| $Ni_3N$ | 990 F $g^{-1}$ | 50%, 2000 | 6 M KOH | | | [82] |
| $Ni_3N$/graphene<br>rGO//$Ni_3N$-G | 2087.5 F $g^{-1}$<br>142.1 F $g^{-1}$ | 80%, 5000 | 6 M KOH | 50.5 Wh $kg^{-1}$ | 800 W $kg^{-1}$ | [83] |
| $W_2N$ | 100 F $g^{-1}$ | 73%, 500 | 1 M KOH | | | [84] |
| MON micropillar | 0.74 F $cm^{-2}$ | 80%, 4000 | 1 M KOH | | | [85] |
| Nanoporous/nanotubular $VO_xN_y$ | 250 F $g^{-1}$ | >80%, 1000 | 6 M KOH | | | [86] |
| W(O,N) | 85 F $g^{-1}$ | | 1 M $H_2SO_4$ | | | [87] |
| Ti(O,N) | 95.3 F $g^{-1}$ | 72%, 2000 | 1 M KOH | | | [88] |
| MOW(O,N) | 124 F $g^{-1}$ | 46%, 5000 | 1 M $H_2SO_4$ | | | [89] |
| Cellulose nanofibril-rGO-MON | 680 F $g^{-1}$ | | | 114 Wh $kg^{-1}$ | 442 W $kg^{-1}$ | [123] |
| TiN-MON//TiN-$MnO_2$ | 75.1 mF $cm^{-2}$ | 84.5%, 8000 | PVA-KOH | 23.7 μWh $cm^{-2}$ | 8.84 mW $cm^{-2}$ | [85] |
| WON NW//$MnO_2$ | 2.73 F $cm^{-3}$ | 95.2%, 10000 | PVA-LiCl | 1.27 mWh $cm^{-3}$ | 0.62 W $cm^{-3}$ | [125] |

NTA: Nanotube arrays; NWA: Nanowire Arrays; NF: Nanofibers; 2E: two-electrode system; NG: nitrogen doped graphene; APDC: activated polyaniline derived carbon; PC: porous carbon; LIC: Lithium-ion capacitor; EC/DEC: ethylene carbonate/diethyl carbonate; //: asymmetric configuration; OMC: ordered mesopore carbon

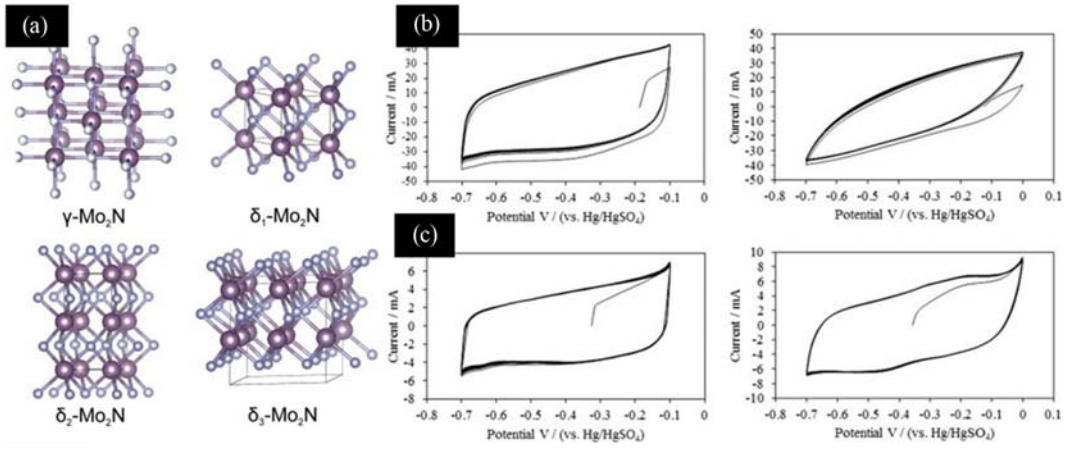


**Fig. 3. (a) Phases of $Mo_2N$; (b) cyclic voltammogram (CV) of $Mo_2N$ derived from chlorimide in 0.5 M $H_2SO_4$ (left) and 0.5 M $K_2SO_4$ (right); (c) CV of imide-derived $Mo_2N$ in 0.5 M $H_2SO_4$ (left) and 0.5 M $K_2SO_4$ (right) (reproduced with permission from Ref. [92] Copyright 2014; Elsevier).**

after nitridation of Mo films over its prior nitridation state or as-deposited Mo oxide [91]. It also exists in several phases like $\alpha$-$Mo_2N$, $\beta$-$Mo_2N$, cubic $\gamma$-$Mo_2N$ or hexagonal $\delta$-$Mo_2N$, but most studied nitrides were $\gamma$- and $\delta$-phase (Fig. 3(a)) [92]. Additionally, Molybdenum nitride with various shapes such as $\gamma$-$Mo_2N$ [28], hunk-like $Mo_2N$ [30], mesoporous $Mo_3N_2$ nanowire [32], porous $Mo_2N$ nanobelts [29], mesoporous $Mo_2N$ nanobelts [93] have been explored in this aspect. Precisely, (111) orientated $\gamma$-$Mo_2N$ was demonstrated for its outstanding supercapacitive characteristics with a volumetric capacitance of 722 F $cm^{-3}$, stability of 100% after 2,000 cycles and relaxation time constant of 200 ms [94].

The charge-storage mechanism of molybdenum nitride relies on both electric double layer capacitance and Faradic pseudocapacitance, depending on the nature of electrolyte as well as the

phase [23,92]. For example, $Mo_2N$ derived from $MoCl_5$ exhibited mainly a double layer capacitive behavior, whereas those obtained from $Mo(NMe_2)_4$ provided a strong signature of redox reaction and higher capacitance in both $H_2SO_4$ and $K_2SO_4$ electrolytes (Fig. 3(b)-(c)) [92]. It has also been reported that the charge storage mechanism of molybdenum nitride in $H_2SO_4$ medium follows two steps: proton involvement in Mo reduction (Eq. (1)) and oxy/hydroxy redox coupling in hydrolyzed Mo (Eq. (2)) [23].

$$Mo^{3+}+N^{3-}+H^{+}+e^{-}\rightleftarrows Mo^{2+}+NH^{2-} \quad (1)$$

$$Mo^{3+}\cdot O^{2-}\cdot OH^{-}+H^{+}+e^{-}\rightleftarrows Mo^{2+}(OH^{-})_2 \quad (2)$$

Nevertheless, it has been reported that the pseudocapacitance of $\gamma$-$Mo_2N$ is dominated by $H^+$ species in 1 M $H_2SO_4$ medium [28]. About two-electrons transfer for every $H^+$ ion involvement for the $\gamma$-$Mo_2N$ in $H_2SO_4$, and a stable operating window was found in the range of −1.2 to 0 V vs $Hg/HgSO_4$ [95]. The maximum theoretical capacitance was estimated to be 1,560 F $g^{-1}$ [95]. However, experimentally obtained values were far beyond the theoretical values, which was attributed to the suppressed adsorption of protons by the oxygen-rich passivation layer [95]. However, the problem associated with poor rate capability, non-ideal cycle behavior and lower specific capacitance has to be overcome by designing suitable structures. Loading tantalum oxide [96] or $Co_3MO_3N$ [31] on $\gamma$-$Mo_2N$ was adopted as a promising approach for enhancing the supercapacitor behavior. However, an excessive amount of Co loading can lead to a distorted and defective $\gamma$-$Mo_2N$ structure, which results in reduced charge storage capacitance [31].

**2. Titanium Nitride (TiN)**

Besides its oxide counterpart, TiN has attracted tremendous at-

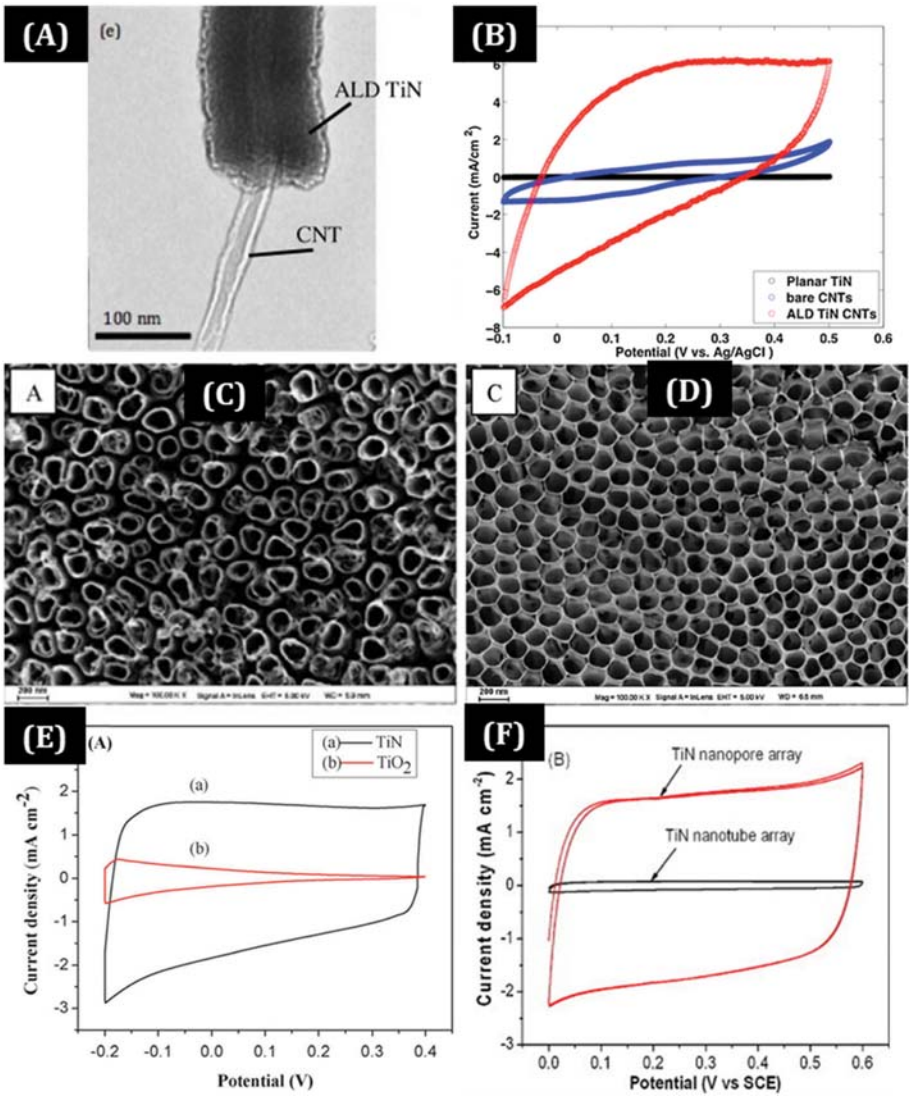


**Fig. 4. Morphology and cyclic voltammogram of (A)-(B) ALD-TiN on CNT, (Reproduced with permission from Ref. [36]. Copyright 2016; Elsevier). Morphology of (C) TiN nanotube arrays and (D) TiN nanopore arrays (Reproduced with permission from Ref. [22] Copyright 2013; Elsevier). Cyclic voltammogram of (E) TiN and $TiO_2$ nanotube arrays (Reproduced with permission from Ref. [45] Copyright 2014; Royal Society of Chemistry), and (F) TiN nanopore and nanotube arrays (Reproduced with permission from Ref. [22] Copyright 2013; Elsevier).**

tention as a supercapacitor electrode material. Moreover, controlling the surface area and particle size of TiN by a metathesis reaction, which are significant parameters for electrodes, resulted in a notably higher capacitance and 100% Coulombic efficiency [97]. To increase the surface area for easy ion-diffusion and electronic transport, synthesizing TiN nanotube arrays is promising. Strikingly, well-aligned TiN nanotube arrays outperformed with capacitance of 83 mF $cm^{-2}$ compared to planar TiN (0.3 mF $cm^{-2}$) (Fig. 4(A)-(B)) [36]. Furthermore, better charge storage properties have been observed in TiN nanotube arrays compared to $TiO_2$ nanotube arrays [45]. The morphology of TiN nanotube and nanopore arrays are shown in Fig. 4(C) and 4(D), respectively. The cyclic performance of TiN nanotube array compared to its oxide counterpart is depicted in Fig. 4(E). However, the issue of poor capacitance retention in TiN nanotubes was observed and attributed to the surface oxidation and structural pulverization. The issue was tackled by implementing a PVA-KOH gel electrolyte instead of KOH electrolyte [98]. The performance was further enhanced by architecting nanopore arrays instead of nanotube arrays, because they offer more accessible surface area (Fig. 4(F)) [22]. However, the nitridation temperature to prepare TiN nanowire arrays from $TiO_2$ nanowire arrays was found to be influential obtaining improved electrical conductivity and higher capacitance [98]. In addition, it has been claimed that a proton acidic electrolyte is more suitable for TiN electrode in terms of capacitance, electrolyte resistance and charge-transfer resistance [22]. Although TiN is envisioned as a promising benchmark for pseudocapacitor electrodes in the nitride family, it has a tendency to be oxidized in an aqueous solution via the following reaction [99];

$$TiN+2H_2O \rightarrow TiO_2+1/2\ N_2+4H^++4e^- \quad (3)$$

$$TiN+3H_2O \rightarrow Ti(OH)_3+N_2+3H^++3e^- \quad (4)$$

Fabricating a composite with carbon nanostructures or designing a core-shell structure is highly promising. The geometry of the electrode materials also has a significant impact on the charge storage properties [36,100]. This has proven by a conformal coating of TiN on CNT [36] or a porous silicon matrix [100]. The TiN coating on

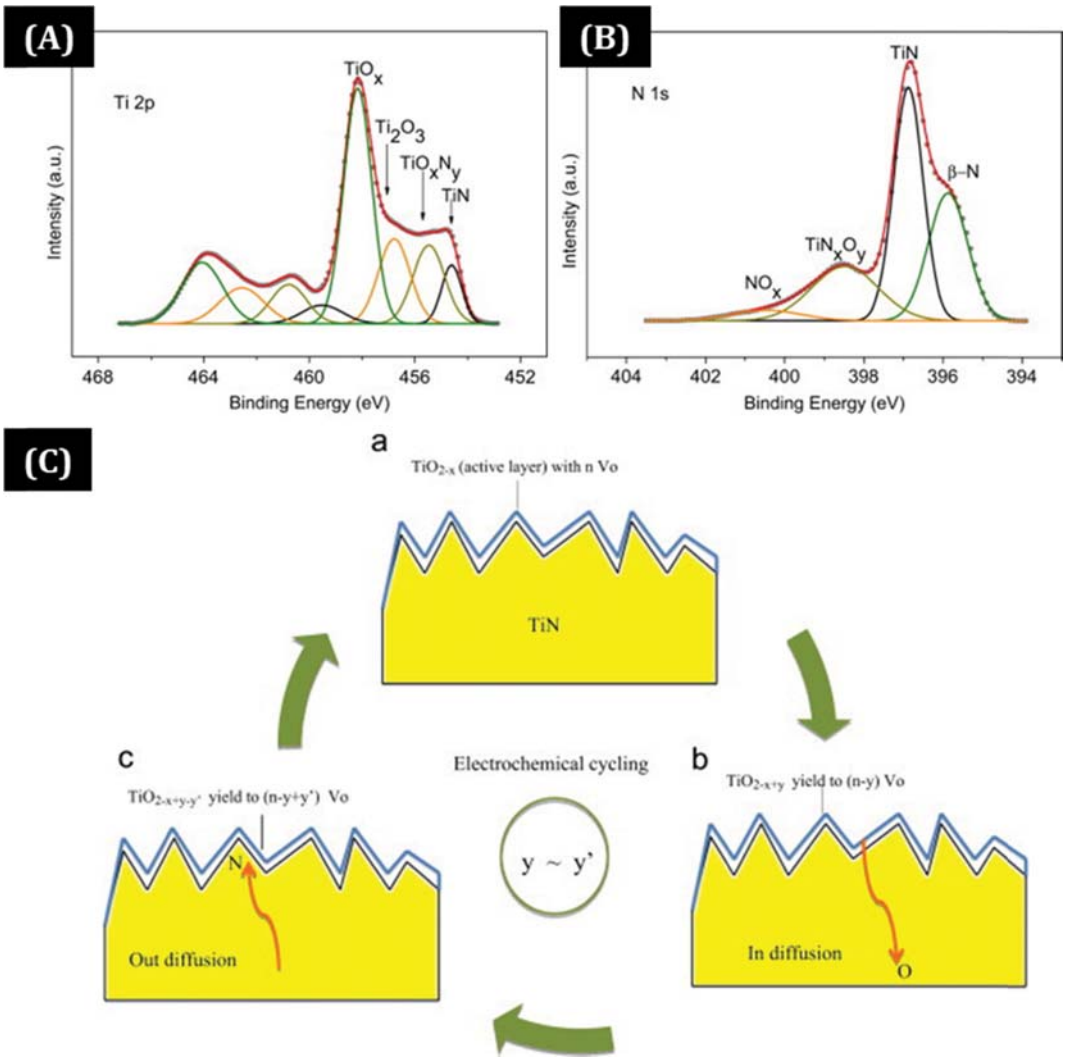


**Fig. 5. High resolution X-ray photoelectron spectra of (A) Ti 2p and (B) N1s, (C) Mechanism for the electrode stability over electrochemical cycle test (Reproduced with permission from Ref. [35] Copyright 2014; Elsevier).**

CNTs demonstrated a capacitance of around 400 times higher than the planar TiN electrode [36]. While around a 360-fold enhancement has been observed for the cauliflower TiN structure on vertical CNTs [35]. The high performance of TiN on CNTs was attributed to the higher accessible surface area, increased oxygen vacancies on the TiN surface and high nitrogen concentration (Fig. 5(A)-(C)) [35,36]. Detailed investigation revealed that the high stability of this composite structure during numerous charge-discharge cycling was due to the balance between oxygen vacancies ($\beta$-N) and substitutional nitrogen, while the total number of oxygen vacancies remained the same (Fig. 5) [35]. Later, a three-fold enhancement in capacitance was demonstrated by diffusing the excess amount of $\beta$-N dopant via vacuum annealing [101].

Since then, several attempts have been implemented considering the advantages of TiN electrode materials. One direction for improving supercapacitor performance was via surface oxidation. Electrochemical oxidation was found to be effective to increase the capacitance rather than the thermal oxidation [102]. The coating of $MoN_x$ on TiN nanotube arrays, by electrochemical deposition and subsequent one-step nitridation process, was found to enhance the capacitance by nearly two-times [50]. The improvement was accomplished with increased surface area, high electrical conductivity and low solubility of $MoN_x$ in an alkaline medium, after the coating. In this case reversible ion adsorption/desorption takes place at the interface and the TiN nanotube array contributes to the double layer capacitance. However, the author claimed that the double layer capacitance was fully responsible for the charge storage mechanism of $MoN_x$/TiN nanotube arrays instead of pseudocapacitance mechanism [50]. But, the point to be noticed here is that the $MoN_x$ was peeled out from the top surface of the TiN nanotube arrays after 1400 charge-discharge cycles [50]. The electroactivity and conductivity of the TiN electrode was further enhanced by designing a hybrid with a coaxial coating of $MnO_2$ [38], polyaniline [44], polyaniline/carbon [46], phosphomolybdic acid/polyaniline [48], polyaniline/$MnO_2$ [49] and $Ni(OH)_2$ [40] on TiN. Even further enhancement was achieved by phosphomolybdic acid ($PM_{O12}$) incorporation to PANI/TiN composite because $PM_{O12}$ promotes the doping-dedoping of PANI [48]. In the case of $MnO_2$/TiN co-axial electrode, a two-step reduction process of $MnO_2$ occurred in an alkaline medium via $Mn^{4+}$ to $Mn^{3+}$ electrochemically followed by $Mn^{3+}$ to $Mn^{2+}$ and the pseudocapacitor contribution of $MnO_2$-TiN dominated over the double layer contribution. However, an increased amount of $MnO_2$ loading could reduce the electrochemical performance, since the pores get filled by $MnO_2$ resulting in lower capacitance [38]. Although the obtained specific capacitance of 2,680 F/g was attractive for a core-shell TiN@$Ni(OH)_2$ nanowire arrays, almost 80% capacitance loss within 250 cycles compelled to focus on finding an alternative strategy [40]. It is noticeable that TiN has poor electrochemical stability in an aqueous medium (Eqs. (3) and (4)). To circumvent this issue, carbon nanostructure was coated on the TiN nanowire, followed by subsequent PANI decoration. With the advantageous features of high conductivity,

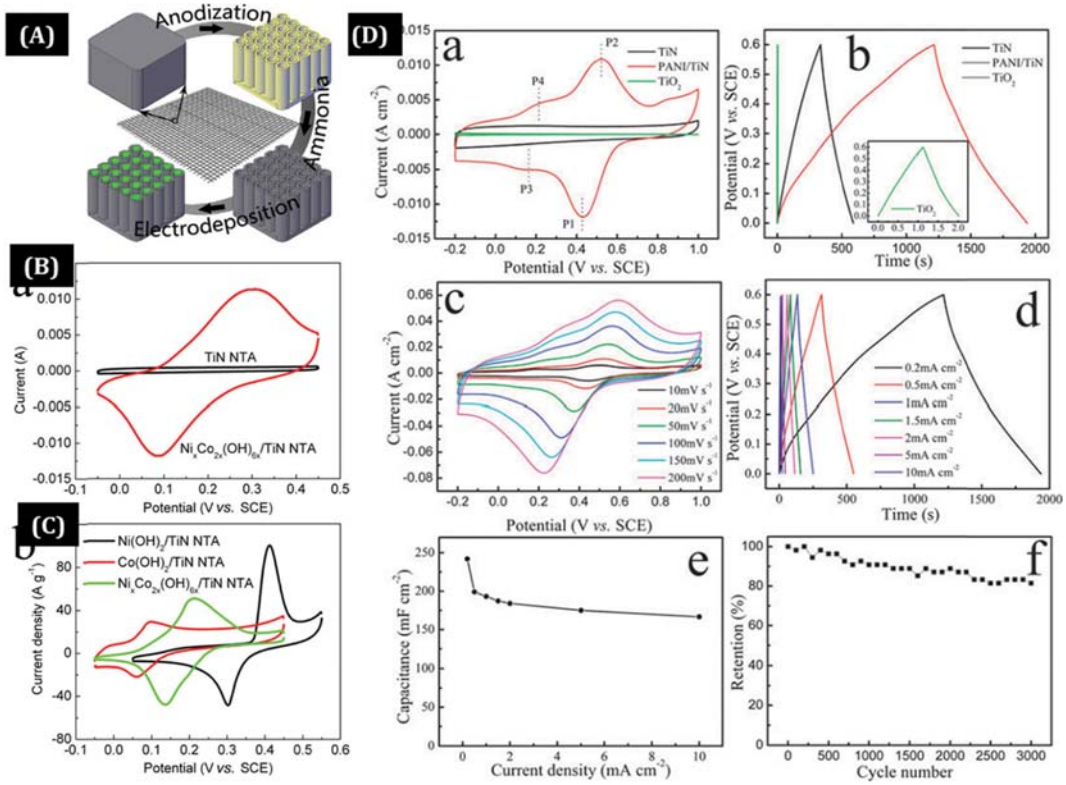


**Fig. 6. (A)-(C) Fabrication schematic and cyclic voltammogram of Coaxial $Ni_xCo_{2x}(OH)_{6x}$/TiN Nanotube Arrays for supercapacitor electrode (Reproduced with permission from Ref. [41] Copyright 2013; American Chemical Society), (D) electrochemical performance of PANI coated TiN electrode (Reproduced with permission from Ref. [43] Copyright 2013; Royal Society of Chemistry).**

structural stability and excellent conducting pathways, core-shell structures have drawn significant attention [21]. In the shell-shell-core nanostructure of PANI/carbon/TiN nanowire arrays, the TiN core with a carbon shell provides an excellent electron transport path, the carbon shell protects the TiN from corrosion and the PANI shell contributes a high pseudocapacitance [46]. Moreover, the carbon shell formation via glucose-assisted hydrothermal method results in an increase of the capacitance retention from 9.1% to 95% after 15,000 cycles [42].

Eventually, TiN nanotube/nanowire arrays were also implemented as a more suitable substrate than its oxide counterpart to obtain high capacitance performance of $Ni_xCo_{2x}(OH)_{6x}$ [41], polyaniline [43], polypyrrole [45], porous silicon [100] and so on (Fig. 6(A)-(D)). The superiority of self-standing nanotube/nanowire arrays includes (i) a highly accessible surface area to an electrolyte, (ii) a conductive framework for feasible electron transport, (iii) binder-free and conductive agent-free electrode material, and (iv) excellent rate capability of bimetallic hydroxides or conducting polymers. The importance of nanotube arrays as substrate was also proven by comparing an experimental investigation with TiN film [41]. Impressively, TiN improved the wettability, electrical conductivity and electrochemical stability in electrolyte media when coated on porous silicon matrix [100]. Moreover, TiN modified lithium titanate has been explored as lithium-ion-capacitor electrode, and the performance was found to depend on the degree of nitrogen doping as well as the TiN coating thickness [39]. Remarkably, the ability of a TiN modified lithium titanate electrode can operate at a higher potential window of up to 2.4 V in an aqueous LiOH electrolyte [39]. To increase the energy density further, protic ionic liquid electrolytes have been implemented. The potential window was extended up to 2 V using an ionic electrolyte, but a higher equivalent series resistance and almost similar capacitance was obtained compared to $H_2SO_4$ electrolyte [103]. Moreover to improve the energy density, an asymmetric device, made of $Fe_2N$-$Ti_2N$ core shell, was demonstrated to operate at a higher potential window of 2.0 V. The $Ti_2N$ shell played dual role in the core-shell structure: shape-preserved conversation from FeOOH to $Fe_2N$ conversion and excellent retention of a nanorod structure over repeated charge-discharge cycles. The authors also anticipated the pioneering can be extended to other metal nitrides, namely, SnN, AlN, $Zn_3N_2$ and $Mg_3N_2$ [21].

### 3. Vanadium Nitride

Vanadium nitride is another promising nitride that opens up new prospects as supercapacitor electrode material, owing to its various oxidation states (II-V), good electrical conductivity ($1.7\times10^6\ \Omega^{-1}m^{-1}$), high melting point (2,300 K), good thermal stability and wide operation window in negative potential (Fig. 7(A)) [104]. Hence, a great deal of attention has been paid to a VN-based supercapacitor electrode due to its high capacitance of 1,340 F $g^{-1}$ [105]. The material itself acts as a core-shell composite [59]. However, the practical value is far from the experimentally obtained capacitance, and hence significant research attention is being given to this material. Nanostructured VN powders, prepared by two-step ammonolysis reaction at 1,000 °C, showed an electrode-electrolyte interfacial charge density of 6.65, which is much higher than that of a carbon-based double layer capacitor (0.17-0.2). In addition, the obtained high bulk charge density of 0.691 indicates that more than a half of vanadium metals experience redox reac-

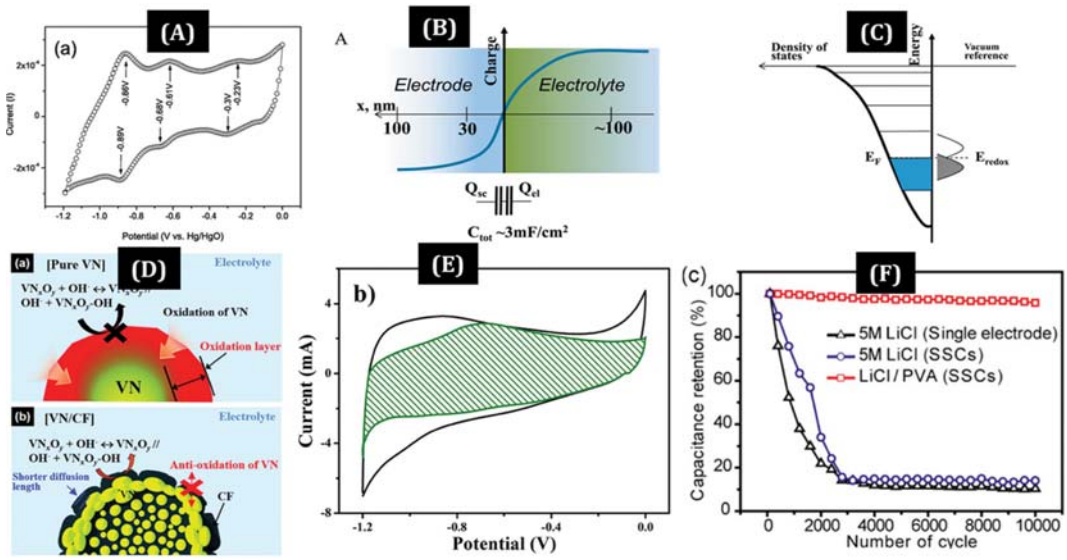


**Fig. 7. (A) CV of VN powder electrode (Reproduced with permission from Ref. [112] Copyright 2018; Elsevier), (B) Charge storage at electrolyte-semiconductor interface for the VN thin film (Reproduced with permission from Ref. [108] Copyright 2016; Elsevier), (C) position of the electrode's Fermi level w.r.t. the redox potential of electrolyte as film thickness varies (Reproduced with permission from Ref. [108] Copyright 2016; Elsevier), (D) Charge storage mechanism of VN and VN-carbon fiber composite (Reproduced with permission from Ref. [62] Copyright 2017; Royal Society of Chemistry) (E) CV of core-shell VN-carbon composite, where shaded region contributed from double layer formation and rest is due to redox reaction (Reproduced with permission from Ref. [65] Copyright 2018; Elsevier), (F) Capacitance retention with respect to the electrolyte (Reproduced with permission from Ref. [58] Copyright 2013; American Chemical Society).**

tion [55]. Increasing the surface area and pore size in a nanometer regime was found to be effective towards enhancing the capacitance of materials. However, the capacitance of VN was inversely related to the particle size [106,107]. It is unfortunate that the nanocrystalline VN suffers from cycle-induced capacitance loss due to formation of oxide layer at the surface [54,105]. Conversely, the capacitance of VN thin film had an increased cycling performance due to surface impregnation by the electrolyte with time. An opposite trend was observed for the powder samples because they got dissolved in the electrolyte [56]. The film thickness of 60 nm was found to be crucial in this study. Below this thickness, film was insufficient to promote the electron transfer and was affected by oxidation [56]. It has been reported that the space charge accumulation mechanism takes place in the oxygen-free VN film instead of reduction in vanadium cations by the hydroxyl group [108]. The study on film thickness dependent capacitance showed an active subsurface layer with a charge-accumulating effective thickness of up to 100 nm, as shown in Fig. 7(B)-(C), where the charge screening length was about 30 nm [108]. To increase the surface area, shorten the diffusion path of the electrolyte ions and in-turn enhancement in the specific capacitance, VN was grown on graphite foam [109]. However, the planar structure and agglomeration of the materials after several charge-discharge cycles created an unfavorable performance in the supercapacitor. Hence, the self-supported vertical structure can mitigate the above-mentioned deficiencies. Encouragingly, electrospun porous VN hollow nanofibers were realized as a better electrode by virtue of their 1D texture and the presence of numerous porous particles [57]. Nevertheless, the process temperature in electrospinning method needs be optimized. Regrettably, there was around 46% capacitance fading after 1,000 cycles due to a thick oxide layer formation on the surface [57]. Porous VN nanowires also suffered from the same instability after cycling measurement in an aqueous electrolyte (LiCl). It was ascribed to the irreversible oxidation reaction, irreversible phase change and nanowire detachment from the substrate during process [58].

The limited rate capacitance and the problem associated with oxide layer formation were encountered by combining VN with carbon structures (Fig. 7(D)) [64-66,110]. The VN-nitrogen doped carbon with a high surface area of 2,400 $m^2\ g^{-1}$ was prepared by adding cesium acetate and zinc acetate as porogens [111]. Interestingly, VN quantum dot/nitrogen-doped microporous carbon composites, prepared by electrospun method, exhibited a higher capacitance of 403.5 F $g^{-1}$ along with a capacitance retention of 75.3% after 1,000 cycles [61]. The *in-situ* preparation of core(carbon)-shell(VN) nanosphere using metal-organic self-assemblies also showed outstanding supercapacitive behavior. The optimized loading of VN into the core-shell structure is essential to obtain the best capacitive properties in terms of specific capacitance, electrochemical efficiency and diffusion ability [65]. The charge storage of this core-shell structure was 28% from reversible redox reaction of vanadium oxidation states (II, III, IV and V) as well as 72% from the double layer formation due to hydroxyl absorption through the following equation (Fig. 7(E)) [65]:

$$VN_xO_y+OH^- \rightleftarrows VN_xO_y||OH^- + VN_xO_y-OH \quad (5)$$

$$VN_xO_y+\delta OH^- \rightleftarrows VN_xO_{y+\delta}H \quad (6)$$

In addition to the capacitance retention, the rate performance of the materials is also another key factor for the supercapacitor. Yet, a serious problem with the VN electrode is its poor rate capacitance, although it can provide excellent chare storage capacitance. The capacitance retention was found to depend on the range of potential window. It was also reported that the capacitance retention improved with a reduction in potential from (−1.2 to 0 V) to (−1.2 to −0.3 V) as well as with change in pH of the electrolyte from 14 to 12 [105]. It has also been suggested that VN should be cycled between −0.4 to −1.0 V *vs* Hg/HgO to avoid the degradation of the electrode as well as the electrolyte [104]. The electrode material was found to unstable and self-discharged by dissolved oxygen in electrolyte above −0.4 V [104]. On the other hand, the absence of $V^{5+}$ oxidation state in VN, synthesized by milling induced mechano-chemical reactions in Ref. [107], exhibited an excellent cycling performance even though the capacitance was very low (25-60 F/g). The poor rate performance in most of the VN-based supercapacitor studies was overcome by adopting another growth strategy. It has been shown that VN nanorods produced by $NH_3$ reduction of $V_2O_5$ exhibited a weak dependence of mass loading on the current collector as well as excellent rate capabilities [59]. The fact was accomplished by the crystalline structure of nitride [59]. Whereas, a fast and reversible redox reaction was considered to be the dominating factor for an improved rate capacitance of VN produced by calcining a vanadium oxide aerogel in $NH_3$ [113].

The choice of an electrolyte and its concentration plays a decisive role in the performance of supercapacitors [56,114,115]. Even a suitable potential window range was found to vary with respect to the choice of aqueous electrolyte [59]. Indeed, a higher electrolyte concentration was found to lower the overpotential for $V^{2+}$ to $V^{3+}$ transformation, decrease the charge transfer resistance and electrolyte solution resistance as well as promote the charge storage kinetics and hence better charge storage performance [115]. The report [28] provided evidence for the pseudocapacitance of VN in 1 M KOH, which mainly relies on the $OH^-$ species and $K^+$ plays a minor role. The reversible redox reactions were clearly observed from the cyclic voltammogram [112]. On the other hand, the redox reaction of oxy-nitride passivated with OH- along with the double layer formation was proposed based on the post-cycling IR and XPS investigation [105]. The result of quartz crystal microbalance studies evidenced the involvement of an oxynitride surface in a neutral electrolyte for the charge storage mechanism of the VN structures [71]. The thickness of oxide layer formation also played a pivotal role in charge storage. The reduction in oxide layer thickness during cycling can lead to a reduction in capacitance. Hence, stabilizing the oxide layer is crucial, and the result showed that $K_2SO_4$ can be used as an electrolyte to obtain higher cyclic stability compared to an alkaline electrolyte [64]. However, an electrochemical investigation of oxygen-free pure VN thin film revealed no role of the $OH^-$ species in charge storage behavior. On the other hand, studies revealed that compatibility of an organic electrolyte for the VN-based supercapacitor obtained a potential window of 2.5 V [109]. Although composite structures of VN could show enhanced capacitance, the core-shell VN-carbon com-

posite failed to retain its capacitance of about 60% after 5000 charge-discharge cycles [65]. We owe thanks to the research group for showing a novel strategy of using a LiCl/PVA gel electrolyte rather than the aqueous electrolyte, which protected the structure from dissolution by minimizing water content and holding the active material with the current collector (Fig. 7(F)). They showed that porous VN nanowires in the LiCl/PVA gel electrolyte (i) retained 95.3% of its initial capacitance even after 10,000 cycles

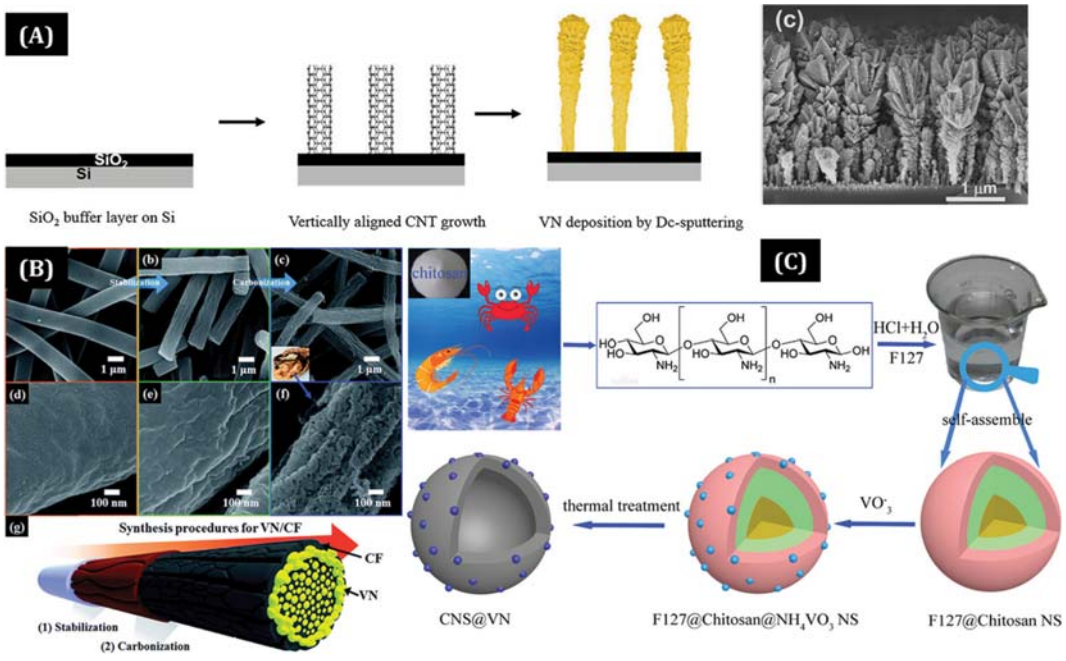


**Fig. 8. Schematic and morphology of VN-carbon composite design by (A) DC-sputtering (Reproduced with permission from Ref. [64] Copyright 2017; Elsevier), (B) electrospinning method (Reproduced with permission from Ref. [62] Copyright 2017; Royal Society of Chemistry), and (C) simple chemistry with carbonization method (Reproduced with permission from Ref. [65] Copyright 2018; Elsevier).**

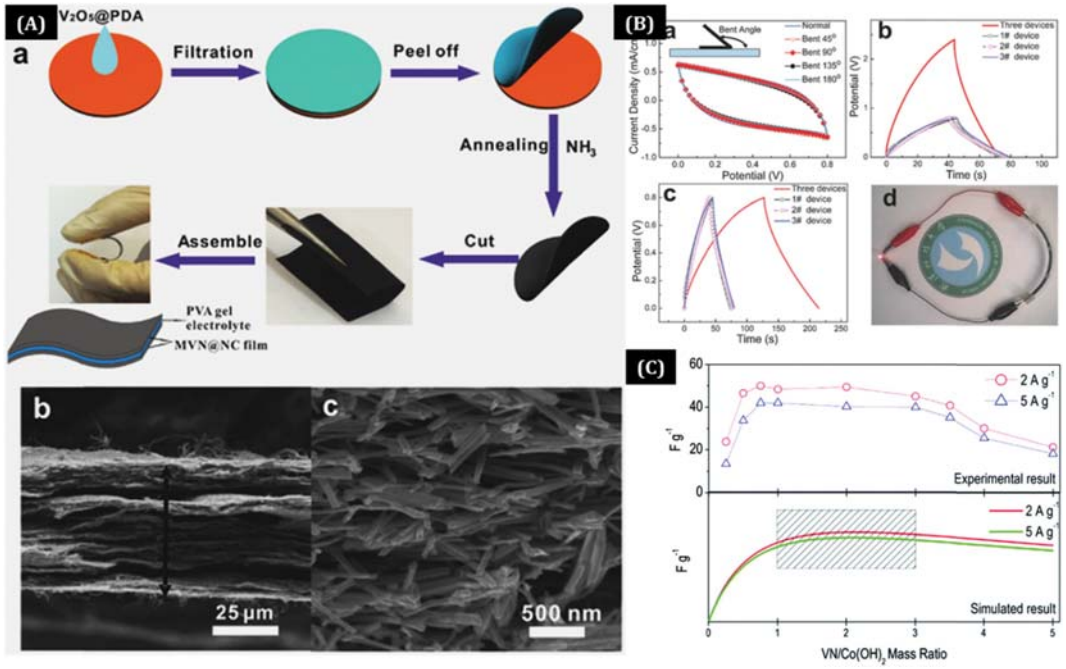


**Fig. 9. (A) Schematic, morphology and (B) performance of nitrogen-doped carbon encapsulated mesoporous vanadium nitride nanowires based solid state device (Reproduced with permission from Ref. [63] Copyright 2015; Wiley), (C) experimental and simulated plot of Specific capacitance with respect to the mass ratio of VN/Co(OH)$_2$ composite (Reproduced with permission from Ref. [69] Copyright 2014; Royal Society of Chemistry).**

without sacrificing capacitive behavior, (ii) had a rapid frequency response (0.27 s for gel electrolyte, while 0.38 s for LiCl) and (iii) preserved the morphology better than in aqueous electrolyte [58]. Moreover, capacitance retention of a VN nanowire//$VO_x$ nanowire asymmetric device was found to depend on the operating potential window. Capacitance retention of the system was 87.5%, 61% and 84% for the potential windows of 1.8, 2 and 2.2 V, respectively.

Significant advances in improving capacitive properties of VN-based materials have been made by integrating the materials into carbon matrix. Some of the strategies and performances are depicted in Fig. 8(A)-(C). A recent effort was made to design a lightweight, flexible and free-standing mesoporous VN nanowires/carbon electrode (Fig. 9(A)-(B)) [63,116]. A fabricated symmetric device exhibited a high-performance supercapacitor with a volumetric capacitance of 7.9 F $cm^{-3}$ and a capacitance retention of 82% even after 10000 charge-discharge cycles [116]. The capacitance performance of VN was further improved by designing a heterostructure like $Co(OH)_2$. Note that, as exhibited in Fig. 9(C), the mass loading of $Co(OH)_2$ has a strong influence on the charge storage performance [69]. Finally, the different specific capacitance values of VN nitride-based materials are due to compositional variation in the surface layer.

## 4. Niobium Nitride

Niobium nitride, another impressive material in the nitride family, has been considered as a promising contender for high-performance supercapacitor applications. In particular, porous NbN was employed as a suitable anode material for a Li-ion hybrid capacitor [117]. Excellent stability was observed for NbN in 1 M KOH, which is notable in comparison to other nitrides [118]. Indeed, NbN nanoparticles served not only as an electrode but also as a preventer of the agglomeration of graphene, which, in turn, improved the charge storage behavior of the composite [119]. Capacitance retention was further improved to 100% after 2000 cycles by integrating the nanochannel structure with a thin carbon coating. On the other hand, NbN/nitrogen-doped graphene composite was also chosen as a suitable anode material to balance the $Li^+$ intercalation/deintercalation rate at the cathode and the adsorption/desorption rate at the anode [119]. However, NbN has a lower

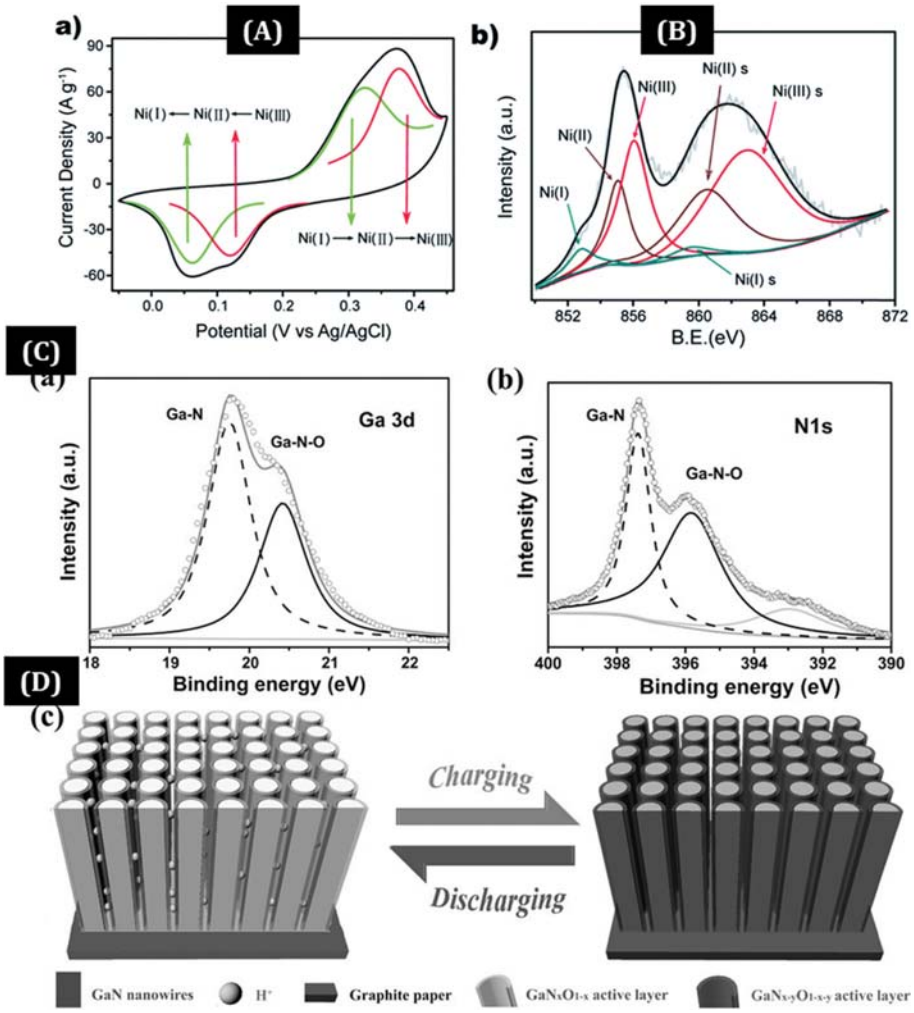


**Fig. 10. (A) Electrochemical performance and (B) Ni2*p* X-ray photoelectron (XP) spectra of $Ni_3N_2$ electrode (Reproduced with permission from Ref. [83] Copyright 2015; Royal Society of Chemistry), (C) high resolution XP spectra of Ga and N1*s* (Reproduced with permission from Ref. [79] Copyright 2017; Wiley), (D) charge storage mechanism of GaN electrode (Reproduced with permission from Ref. [79] Copyright 2017; Wiley).**

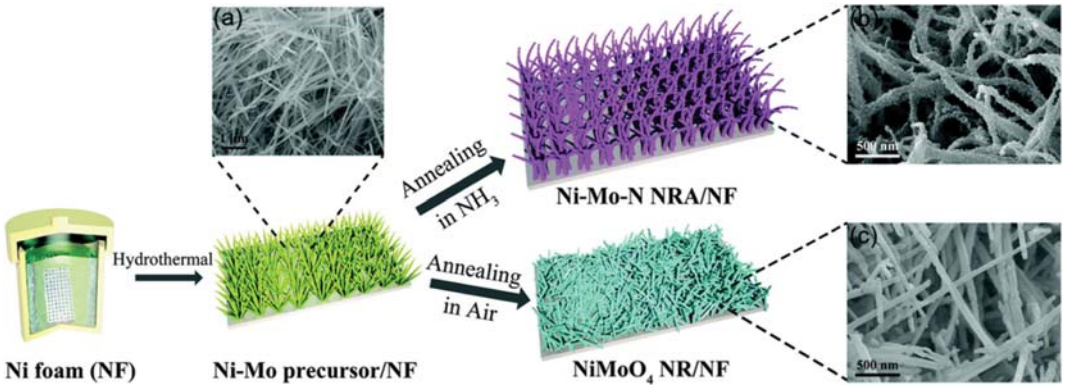


**Fig. 11. Schematic of Ni nanoparticle decorated $Ni_{0.2}Mo_{0.8}N$ arrays and $NiMoO_4$ nanorods electrode fabrication and their corresponding scanning electron micrographs (Reproduced with permission from Ref. [74] Copyright 2017; Royall Society of Chemistry).**

oxidation state (+3) with a lower pseudocapacitance of NbN (73 F $g^{-1}$). For instance, the nitrogen-rich $Nb_4N_5$ phase with high oxidation state of +5 exhibits an impressive areal capacitance of 225.8 mF $cm^{-2}$, capacitance retention of 70.9% after 2000 cycles and 60.8% rate capability from 0.5 to 10 mA $cm^{-2}$. The $Nb_4N_5$ nanochannel was reported to be a promising contender for the supercapacitor electrode (Fig. 10) [75].

**5. Other Nitrides**

Apart from the above-mentioned popular nitrides, other nitrides like RuN [80], CrN [76], CoN [76], LaN [81], $Ni_3N$ [82,83], GaN [79], $Fe_2N$ [21,77], WN [27], $W_2N$ [84] have captured the research interest as electrode materials for high-performance supercapacitor applications. Here, we have only highlighted the significant aspects of nitrides while explored as supercapacitor. Impressively, the CrN//AC and CoN//AC asymmetric device made it possible to operate up to a 3 V potential window in 1 M $LiPF_6$ dissolved in ethylene carbonate/diethyl carbonate [76]. Meanwhile, this study presented a novel strategy of preparing a metal nitride/carbon fiber composite from the waste metal ion-adsorbed cigarette, and it demonstrated an excellent charge storage behavior. Integrated metal nitrides included in the study were VN, $Fe_2N$, $Co_{5.47}N$ and $Ni_3N$ [120]. Even incorporating $Ni_3N$ with graphene not only enhanced the charge storage capacity, indeed it also assisted in improving the cycle stability [83]. This fact was attributed to the smaller size of $Ni_3N$ particles in the graphene matrix, which created a higher accessible surface for a Faradic reaction and minimal volume change [83]. Another well-known nitride in the electronic industry, gallium nitride (GaN) has also been explored as supercapacitor electrode. The electrochemical performance and charge storage mechanism of GaN is illustrated in Fig. 10(C)-(D). The authors of that study believed that the oxynitride layer on nitride surface possessed higher electrical conductivity and enhanced pseudocapacitance [79]. They interpreted the pseudocapacitive charge storage mechanism of the mesoporous GaN membrane was based on the redox kinetics between nitride and oxy-nitride layer via the following reaction [79]:

$$GaN_{1-x}O_x+2\gamma H^++2\gamma e^- \rightleftarrows GaN_{1-x-y}O_{x-y}+2\gamma H_2O \quad (7)$$

Considering the synergetic effect, binary nitrides also came into the limelight as a high-performance supercapacitor electrode. Binary TiVN [73], $Fe_2N$-TiN [121] and VTiN/C nanofibers [72] are examples of that. However, the atomic ratio of two nitrides is crucial to obtain higher performance. For example, TiVN with a 1 : 1 atomic ratio of Ti/V exhibited the highest capacitance of 15 mF $cm^{-2}$ along with high cycling ability of the TiN and the high areal capacitance of the VN [73]. Substantial improvement in the capacitive performance has been observed for VTiN coated on carbon fiber with a specific capacitance of 430.7 F $g^{-1}$ and a higher rate capability compared to the binary counterpart, where the respective specific capacitance of VN/C and TiN/C is 291.5 F $g^{-1}$ and 108.8 F $g^{-1}$ [72]. Moreover, Ni nanoparticles incorporated in Ni-Mo nitride enhanced the areal capacitance to 4.892 F $cm^{-2}$ and it could be adopted as a strategy to obtain high-performance supercapacitor devices [74]. A schematic of fabricating this hybrid structure is displayed in Fig. 11.

## OXY-NITRIDES (O,N) AND THEIR SUPERCAPACITOR PERFORMANCES

Inspired by the metal nitride-based supercapacitor performance, the metal-oxide nitride has also attracted considerable attention towards supercapacitor electrode applications. Although the metal nitride-based supercapacitors are promising, their potential is limited due to poor rate performance and cycle-life. On the other hand, surface oxidation of the nitride materials exhibited better capacitive properties [102]. Note that the presence of oxynitrides on the surface of VN contributes to a redox reaction [62]. Since the wettability of the electrode material is one of the key aspects, materials with hydrophilic nature are well-appreciated for supercapacitor devices. Interestingly, metal oxynitrides possess higher wetting compared to their nitride counterpart [85]. The above-mentioned features bring in a significant research attention on the metal-oxynitride based materials to be used as supercapacitor electrode. A general schematic to prepare metal oxynitride is shown in Fig. 2. In addition, supercapacitive performance of these materials is summarized in Table 1. Till now, molybdenum, titanium, vanadium and tungsten oxynitrides, as well as, bi-metallic oxynitrides have been extensively studied as a supercapacitor electrode [85-89,122-124]. The charge storage of oxynitrides relied on either double layer mechanism or redox kinetics, depending upon the kind

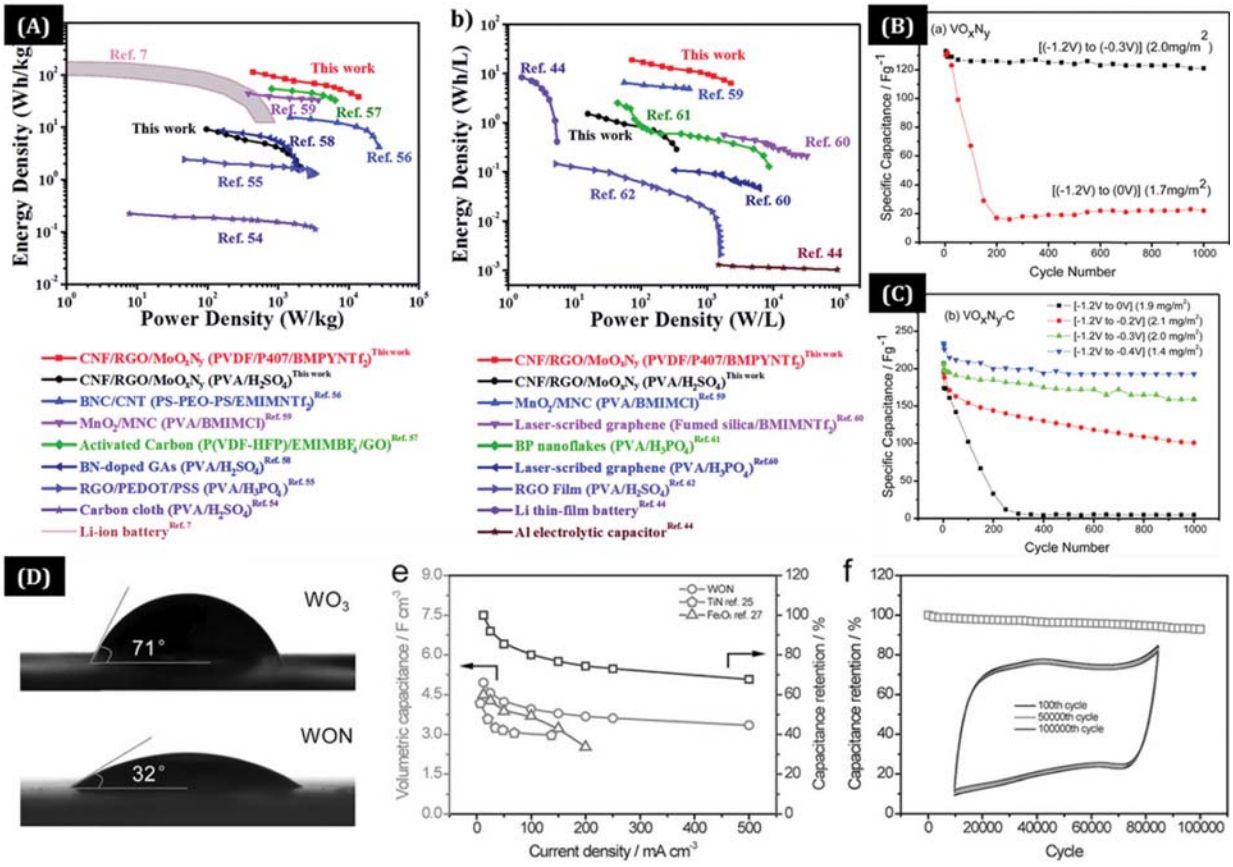


**Fig. 12. (A) Ragone plots of cellulose nanofibril-reduced graphene oxide-$MoO_xN_y$ aerogel in $H_2SO_4$-PVA electrolyte compared to other materials (Reproduced with permission from Ref. [123] Copyright 2017; Royal Society of Chemistry), (B)-(C) Cyclic performance of $VO_xN_y$ and $VO_xN_y$-carbon composite with different potential window in 1 M KOH vs Hg/HgO (Reproduced with permission from Ref. [124] Copyright 2014; Elsevier), (D) wettability, volumetric capacitance and cycle performance of WON (Reproduced with permission from Ref. [125] Copyright 2015; Wiley).**

of metal used [122]. Although existing reports on the oxynitride-based supercapacitor are limited, the state-of-art is covered in the following paragraphs.

Taking advantage of the presence of both oxygen and nitrogen, a facile synthesis process to fabricate molybdenum oxynitride (MON) micropillar was demonstrated [85]. Another key finding of the report [85] is the utilization of MON as an anode material for supercapacitor, where carbon materials are conventionally and extensively used. The obtained specific capacitance in this case was of about 736.6 mF $cm^{-2}$. Noteworthy is that the capacitance was higher than that of $Mo_2N$/TiN due to higher conductivity and higher wettability of MON brought about by nitridation [85]. In most of the cases, metal oxides were undergoing nitridation process for transforming the metal oxides to metal nitride. The nitridation process involves annealing steps at high temperature under $NH_3$ atmosphere. However, usage of $NH_3$ is very unlikely in terms of safety as well as when the cost of material preparation is concerned. In this scenario, using $N_2$ gas for nitridation is an appropriate alternative. Additionally, the nitridation of $MoO_3$ in a $N_2$ environment resulted in a lower percentage of conversion from oxide to nitride with a better charge storage behavior compared to the nitridation in a $NH_3$ environment [20]. However, the nitridation temperature played a pivotal role determining the electrode performance [20]. The partial conversion of oxide to nitride also was well-supported from the electrochemical investigation of dual nitrogen-doped $MoO_3$. It has been shown that the linear capacitance of $MoO_3$, N-$MoO_{3-x}$ and MoN nanowires was 7.6, 31.6 and 13.7 mF $cm^{-1}$ [90]. Recently, a porous and free-standing cellulose nanofibril-reduced graphene oxide-$MoO_xN_y$ aerogel was fabricated by freeze-drying and in-situ hydrazine reduction to obtain ultra-high energy density (Fig. 12(A)) [123]. An excellent performance was exhibited by aerogel-based solid-sate supercapacitor compared to the energy density and cycle life of Li-ion battery [123].

Considerable attention has also been devoted to the nanoporous/nanotubular vanadium oxynitrides [86,122]. Point to be noted here is that a binder-free, current collector free and conducting additive-free electrode was synthesized via simple anodization of vanadium foil in a $[BF_4]^-$ electrolyte [86]. The charge-storage mechanism here relied upon the redox kinetics in KOH medium [122]. However, like VN, the $VO_xN_y$ also suffered from an undesirable capacitance retention owing to an increase in oxide layer, irreversible oxidation of the electrode material and its dissolution in electrolyte [124]. It has been reported that choosing an operation potential range in the KOH medium can eliminate the negative effect of

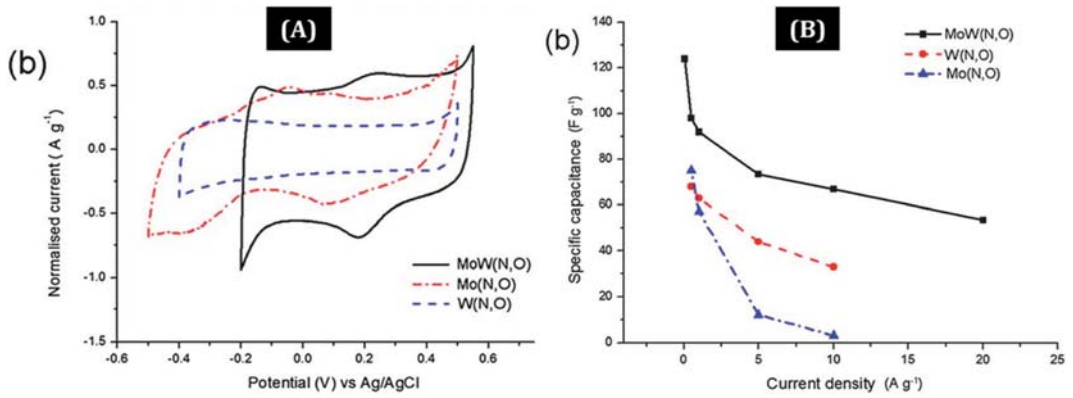


**Fig. 13. Specific capacitance of bimetallic MoW(N,O) compared to their monometallic counterpart (Reproduced with permission from Ref. [89] Copyright 2013; Royal Society of Chemistry).**

retention (Fig. 12(B)-(C)). In particular, both the $VO_xN_y$ and $VO_xN_y$-carbon composites exhibited excellent cycle performance within the potential range of −1.2 V to −0.4 V in KOH medium with respect to the Hg/HgO [124].

Owing to the maximum valence electrons as occupied by nitrogen and oxygen in interstitial sites of tungsten oxynitrides, W(O,N), it was recognized as an another promising supercapacitor electrode material [87,125]. Apart from these, the W(O,N) also has excellent electrical conductivity, thermal stability, high melting point, biocompatibility and chemical inertness. Eventually, holey W(O,N) nanowires exhibited better wettability (contact angle of $32^0$) than their oxide counterpart ($71^0$) (Fig. 12(D)). Noteworthy is that the electrode materials exhibited excellent chemical and mechanical stability even after 10000 charge-discharge cycles, as evidenced from XPS investigation [125]. The electrochemical investigation on mesoporous W(O,N) indicated that the $H_2SO_4$ electrolyte provides highest capacitance, while maximum stability of the material was found in KOH medium among the range of aqueous electrolytes (1 M $H_2SO_4$, 1 M KOH, 3 M KCl, 3 M NaCl, 1 M LiCl and 1 M $CaCl_2$) [87]. The result of lower stability in $H_2SO_4$ was evidenced from the XPS investigation that the progressive oxidized layer formation occurred on the surface while $H_2SO_4$ was used as an electrolyte [87]. A detailed XRD investigation demonstrated that the charge storage mechanism of $W_{0.75}$(N,O) was due to the pseudocapacitive adsorption of cations rather than the bulk intercalation [87].

In spite of the significant advances in capacitive performance of oxy-nitride materials, the important factors, which can affect their electrochemical capacitance performance, are ageing and passivation [126]. The redox peak has been observed in the cyclic voltammogram for the passivated W(O,N), which is a feature of amorphous mesoporous $WO_3$. In spite of a decrease in Coulombic efficiency, an increase in capacitance has been observed. Additionally, the intrinsic conductivity and rate performance were not influenced by the ageing process. This result was attributed to the water splitting and hydrogen evolution around −0.4 V *vs.* Ag/AgCl. Unlike W(O,N), aged Mo(O,N) exhibited better rate performance (17.2% capacitance retained upon increasing current density from 0.5 to 20 A $g^{-1}$) and reduced IR drop in discharge profile while compared with fresh sample (2.7% at 20 A $g^{-1}$) [126]. On the other hand, surface area was reduced and the ratio of $W^{6+}/W^{\delta+}$ was also increased for the passivated W(O,N) upon ageing time. The complete investigation concluded the effect of passivation and ageing depends on the material itself [126]. One should also be careful in controlling the surface area, porosity, surface state and miscellaneous physical properties of the electrode material [88]. With a goal of enhancing the energy density, researchers adopted the concept of developing bimetallic oxynitride materials. Interestingly, MoW(O,N) had a higher capacitance performance than W(O,N) and Mo(O,N) (Fig. 13) [89].

## ASYMMETRIC DEVICE FABRICATION

As mentioned, an aqueous-based supercapacitor device is more desirable from the technological point of view once cost, safety, environment-friendliness are concerned. In an aqueous-based supercapacitor device, the electrodes generally can be operated at maximum to 2 V while assembled in a symmetric configuration [36]. However, this problem can be circumvented by designing two different electrode materials as positive and negative electrodes in an asymmetric device, and it can operate at more than 2 V in an aqueous electrolyte. Impressively, a maximum potential window of 3.2 V has been achieved using aqueous electrolytes [127]. More details about the construction of asymmetric device can be found from the existing reviews [128,129]. However, the operating potential window also depends upon the electrode material and also their interaction with electrolyte. As mentioned, VN and V(O,N) are the examples where the cyclic stability is dependent on the range of potential window applied during the charge storage process [58,124]. Several attempts have been considered to assemble an asymmetric device using metal nitrides and oxynitrides as electrode materials [30,53,68,125]. Both of the electrode materials can be from the nitride family [53], the combination of nitride and oxide [58,68] or else nitride and carbon-based materials [30]. However, one must pay attention to the mass ratio of both the electrode and the operation voltage window while designing an asymmetric device [69,116]. A recent study on a graphene nanosheet-supported $Fe_2N$//TiN asymmetric supercapacitor assembly showed such promise (Fig. 14). The Faradic reaction mechanism responsible for such a pseudocapacitor device is as follows [53]:

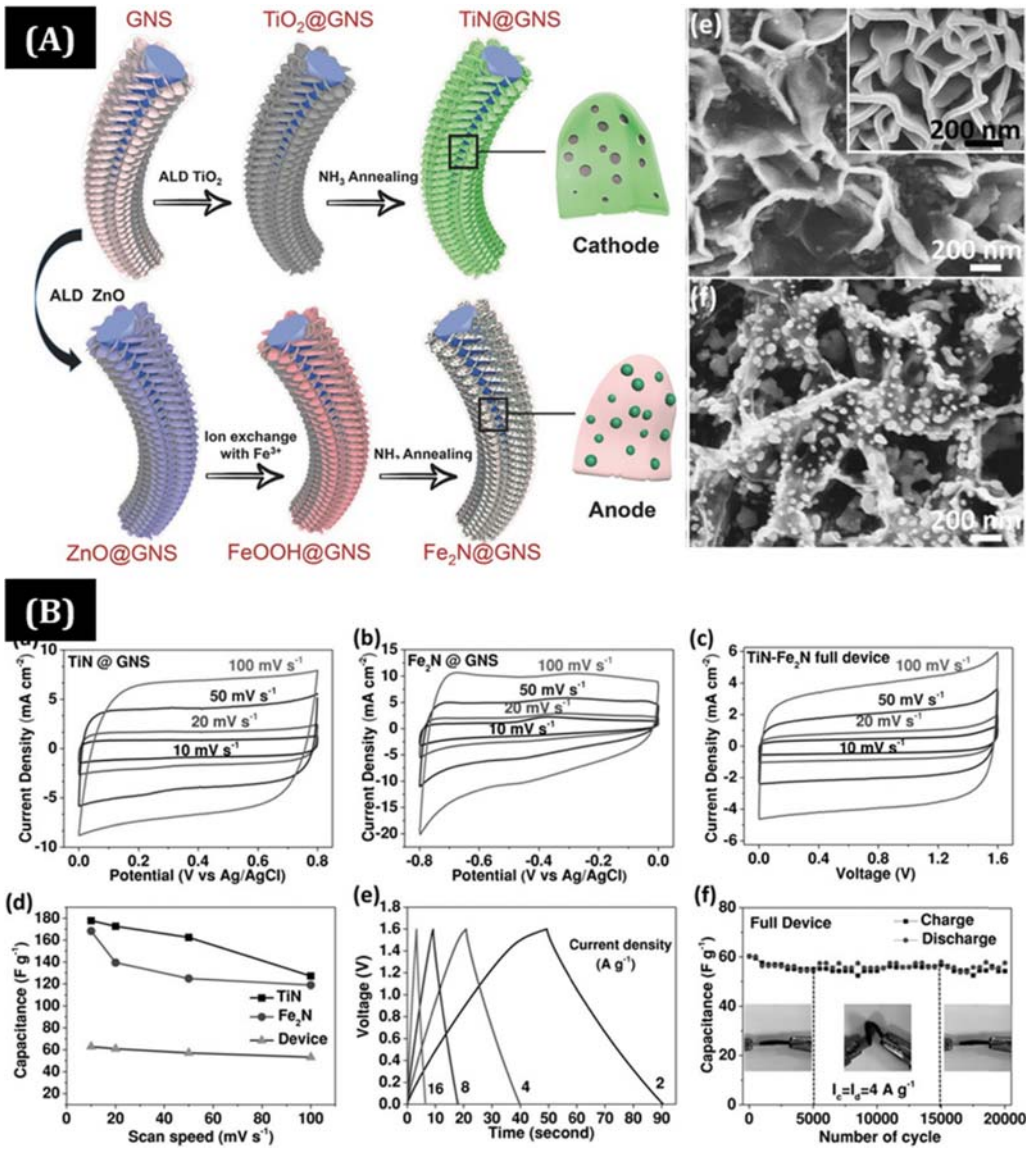


**Fig. 14. (A) Schematic and morphology of TiN@GNS and $Fe_2N$@GNS electrode and (B) its electrochemical performances (Reproduced with permission from Ref. [53], Copyright 2015; Wiley).**

$$Ti_{\frac{3x+2y}{2}}N_xO_y + zLi^+ + ze^- \leftrightarrow Ti_{\frac{3x+2y-z}{4}}N_xO_yLi_z; \quad (8)$$

$$Fe_{\frac{3x+2y}{2}}N_xO_y + zLi^+ + ze^- \leftrightarrow Fe_{\frac{3x+2y-z}{3}}N_xO_yLi_z \quad (9)$$

The valence state of Ti changed from +2 to +4 while that of Fe was from +2 to +3. However, there was also a slight aggregation in $Fe_2N$. Even a wearable asymmetric device made of TiN-MON// TiN-$MnO_2$ demonstrated a superior charge storage performance with a specific capacitance of 75.1 mF $cm^{-2}$ and with 84.5% capacitance retention after 8,000 cycles [85]. An excellent rate capability of 69.6% while current density was increased by 20-fold, more than 95% coulombic efficiency, 95.2% capacitance retention after 10,000 cycles and less than 2% variation in capacitance upon different bending condition have been observed from the W(O,N) based asymmetric device [125]. However, the stable potential window for the W(O,N)//$MnO_2$ was only 1.8 V (Fig. 15). The operating voltage limit in aqueous based asymmetric device compelled considerable research to be conducted in order to improve the energy density [125].

## SUMMARY AND OUTLOOK

We have highlighted the energy storage performance of various metal nitride/oxynitrides materials that are in the limelight of supercapacitor applications. The supercapacitance performance of metal oxides/oxynitrides was summarized in comparison with other nanostructures in Table 2. These nanostructures not only demonstrate remarkable supercapacitive behavior, but also can be used as bridging element for other nanostructure to enhance their electrochemical properties. In addition, metal nitride/oxynitrides are promising as anode materials for asymmetric supercapacitor, where carbon nanostructures are extensively used. Although their super-

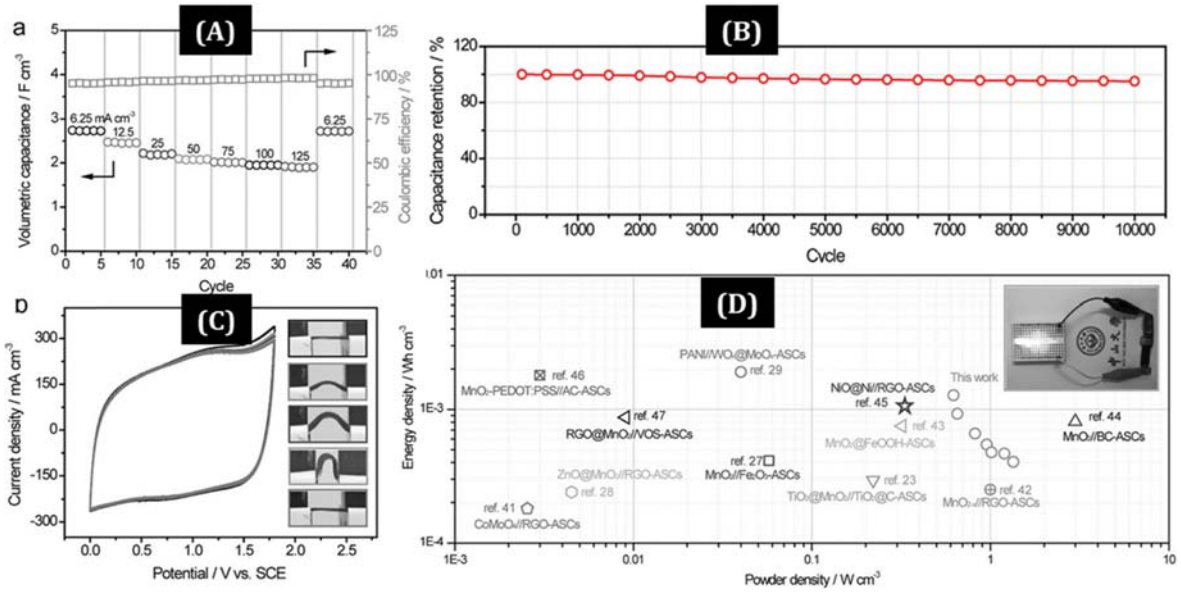


**Fig. 15. (A) Volumetric capacitance and coulombic efficiency, (B) cycle performance, (C) cyclic voltammogram under different bending condition and (D) ragone plot of W(O,N) nanowire//$MnO_2$ asymmetric supercapacitor device (Reproduced with permission from Ref. [125] Copyright 2015; Wiley).**

**Table 2. Supercapacitance performance of metal nitride/oxynitride-based electrode in comparison with other electrodes (parameters for metal nitride/oxynitride is taken from Table 1, parameters for other materials are taken from the cited review article)**

| | Carbon materials | 2D materials | Conducting polymers | Metal oxides/hydroxides | Metal nitride/oxynitrides |
|---|---|---|---|---|---|
| Specific capacitance | | | | | |
| areal (mF cm$^{-2}$) | 0.2-1350 [131,132] | 2.8 -70 [134-136] | | 12-115k [12, 140,141] | 11.8-740 |
| Volumetric (F cm$^{-3}$) | 12-611 [133] | 6.2-900 [134] | | 4.7-305 [140,141] | 15-951.3 |
| Gravimetric (F g$^{-1}$) | 17-556 [131,133] | 2.57-811 [134,137,138] | 30-3000 [139] | 9-2827 [12,140] | 82-990 |
| Energy density | | | | | |
| In unit of Wh kg$^{-1}$ | 5.5-230 [132, 140] | 7.37-186 [142] | 17.2-300 [139, 141] | 0.5-188 [12, 140,143] | 16.5-162 |
| In unit of Wh L$^{-1}$ | 2.5-450 [133] | | | 22 [140] | ~$10^2$ |
| In unit of mWh cm$^{-3}$ | | 16k-110k [134] | 1k-6.16k [139] | | 1-194k |
| Power density | | | | | |
| In unit of W kg$^{-1}$ | 1k-776.8k [140] | 284-106k [138, 142] | 12.1-92.2 [139] | 1.16-400k [12,140,141] | 7.3-54k |
| In unit of W L$^{-1}$ | | | | | ~$3\times10^4$ |
| In unit of mW cm$^{-3}$ | | 11.6- 51k [134, 144] | 40-270 [139] | | 8-328k |

capacitor performance is quite satisfactory, it is still insufficient for realizing their full-phase utilization in commercial appliances. The advantages and challenges are highlighted in Fig. 16. The major shortcomings are a troublesome process, high cost, serious agglomeration during charge-discharge cycling, low yield and so-forth. Considerable research is still needed to bring the nitride-based supercapacitor to a mature level.

(i) Designing a self-supported vertical metal nitride/oxynitride nanostructure via an easy and scalable technique, without use of a binder, conducting additives or a current collector is of great technological interest.

(ii) Based on the existing literature, supercapacitor performance is limited to Ti, V, Mo, Ga, Ru, Cr, Fe, Ni and Co nitrides and Mo, V, Ti and W in oxynitride family. Importantly, all nitrides like $Ta_3N_4$ cannot be used as supercapacitor electrode. The research attention should be on other nitrides like Zn, Al, In, Cu, Mn.

(iii) Since electrolytes play a critical role in the electrochemical behavior of nitrides/oxynitrides, considerable research should be carried out to establish a preferred electrode material and electrolyte combination. The cyclic stability of these structures was improved by aqueous gel type electrolyte instead of aqueous electrolytes. In addition, little attention has been given towards the usage of organic and ionic electrolytes. The investigation on these nanostructures in organic and ionic electrolytes is still a subject of future research.

(iv) The activation process to remove the oxygen-rich passivation layer from the surface can be adopted globally to improve the physical and electrochemical properties [130]. In the context of

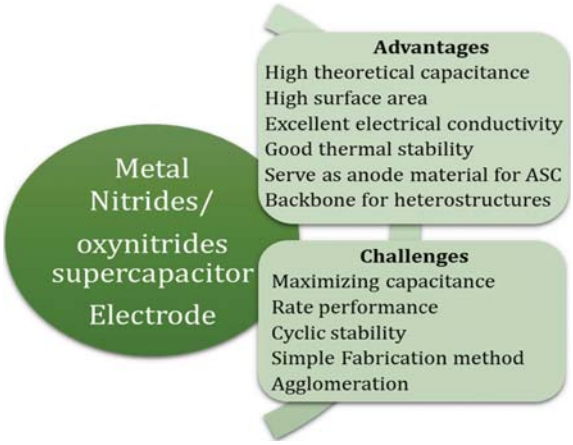


**Fig. 16. Advantages and challenges of metal nitride/oxynitride based supercapacitor electrode material (ASC: Asymmetric Supercapacitor).**

enhancing energy density, doping heteroatoms like S, B, P and nanoparticles can be an effective strategy.

(v) An asymmetric supercapacitor device can provide higher energy density owing to its ability to operate in a high potential window. Proper selection of a pair of cathode and anode materials with a large work function difference, an optimized mass ratio and potential window can further solve the issue of achieving a supercapacitor with high energy density.

With the progress in current materials science research and technological advances, we anticipate the bright prospect of metal nitrides/oxynitrides-based supercapacitor device in near future.

## ACKNOWLEDGEMENT

Subrata Ghosh acknowledges financial support from Basic Science Research Program (2017R1D1A1B03028311) of the National Research Foundation of Korea.

## REFERENCES

1. Z. Lin, E. Goikolea, A. Balducci, K. Naoi, P. L. Taberna, M. Salanne, G. Yushin and P. Simon, *Mater. Today* (2018), DOI:10.1016/j.mattod.2018.01.035.
2. D. P. Dubal, Y. P. Wu and R. Holze, *ChemTexts*, **2**, 1 (2016).
3. A. González, E. Goikolea, J. A. Barrena and R. Mysyk, *Renew. Sust. Energy Rev.*, **58**, 1189 (2016).
4. P. Simon, Y. Gogotsi and B. Dunn, *Science*, **343**, 1210 (2014).
5. L. Xia, L. Yu, D. Hu and G. Z. Chen, *Mater. Chem. Front.*, **1**, 584 (2017).
6. A. Ghosh and Y. H. Lee, *ChemSusChem*, **5**, 480 (2012).
7. S. Ghosh, G. Sahoo, S. R. Polaki, N. G. Krishna, M. Kamruddin and T. Mathews, *J. Appl. Phys.*, **122**, 214902 (2017).
8. A. Thambidurai, J. K. Lourdusamy, J. V. John and S. Ganesan, *Korean J. Chem. Eng.*, **31**, 268 (2014).
9. D. P. Upare, S. Yoon and C. W. Lee, *Korean J. Chem. Eng.*, **28**, 731 (2011).
10. S. Ghosh, S. R. Polaki, P. Ajikumar, N. G. Krishna and M. Kamruddin, *Indian J. Phys.*, **92**, 337 (2018).
11. K. D. Fong, T. Wang and S. K. Smoukov, *Sust. Energy Fuels*, **1**, 1857 (2017).
12. C. Lokhande, D. Dubal and O.-S. Joo, *Curr. Appl. Phys.*, **11**, 255 (2011).
13. N. M. Shinde, A. D. Jagadale, V. S. Kumbhar, T. R. Rana, J. Kim and C. D. Lokhande, *Korean J. Chem. Eng.*, **32**, 974 (2015).
14. E. M. Jin, H. J. Lee, H.-B. Jun and S. M. Jeong, *Korean J. Chem. Eng.*, **34**, 885 (2017).
15. W.-J. Lee, S. Jeong, H. Lee, B.-J. Kim, K.-H. An, Y.-K. Park and S.-C. Jung, *Korean J. Chem. Eng.*, **34**, 2993 (2017).
16. S. Ghosh, B. Gupta, K. Ganesan, A. Das, M. Kamruddin, S. Dash and A. K. Tyagi, *Mater. Today: Proc.*, **3**, 1686 (2016).
17. X. Huang, M. Kim, H. Suh and I. Kim, *Korean J. Chem. Eng.*, **33**, 2228 (2016).
18. N. Venugopal and W.-S. Kim, *Korean J. Chem. Eng.*, **32**, 1918 (2015).
19. X. Lu, G. Wang, T. Zhai, M. Yu, J. Gan, Y. Tong and Y. Li, *Nano Lett.*, **12**, 1690 (2012).
20. Y.-J. B. Ting, H. Wu, N. P. Kherani K. Lian, *Mater. Chem. Phys.*, **154**, 118 (2015).
21. C. Zhu, Y. Sun, D. Chao, X. Wang, P. Yang, X. Zhang, H. Huang, H. Zhang and H. J. Fan, *Nano Energy*, **26**, 1 (2016).
22. Y. Xie, Y. Wang and H. Du, *Mater. Sci. Eng. B*, **178**, 1443 (2013).
23. T. C. Liu, W. Pell, B. Conway and S. Roberson, *J. Electrochem. Soc.*, **145**, 1882 (1998).
24. Y. Zhong, X. Xia, F. Shi, J. Zhan, J. Tu and H. J. Fan, *Adv. Sci.*, **3**, 1500286 (2016).
25. M.-S. Balogun, W. Qiu, W. Wang, P. Fang, X. Lu and Y. Tong, *J. Mater. Chem. A*, **3**, 1364 (2015).
26. S. Dong, X. Chen, X. Zhang and G. Cui, *Coordination Chem. Rev.*, **257**, 1946 (2013).
27. D. Choi and P. N. Kumta, *J. Amer. Ceram. Soc.*, **90**, 3113 (2007).
28. P. Pande, P. G. Rasmussen and L. T. Thompson, *J. Power Sources*, **207**, 212 (2012).
29. J. Liu, K. Huang, H. L. Tang and M. Lei, *Int. J. Hydrog. Energy*, **41**, 996 (2016).
30. W.-B. Zhang, X.-J. Ma, L.-B. Kong, M.-C. Liu, Y.-C. Luo and L. Kang, *J. Electrochem. Soc.*, **163**, A1300 (2016).
31. C. Chen, D. Zhao, D. Xu and X. Wang, *Mater. Chem. Phys.*, **95**, 84 (2006).
32. K. H. Lee, Y. W. Lee, A. R. Ko, G. Cao and K. W. Park, *J. Amer. Ceram. Soc.*, **96**, 37 (2013).
33. P. Yang, D. Chao, C. Zhu, X. Xia, Y. Zhang, X. Wang, P. Sun, B. K. Tay, Z. X. Shen and W. Mai, *Adv. Sci.*, **3**, 1500299 (2016).
34. S. Dong, X. Chen, L. Gu, X. Zhou, H. Xu, H. Wang, Z. Liu, P. Han, J. Yao, L. Wang, G. Cui and L. Chen, *ACS Appl. Mater. Interfaces*, **3**, 93 (2011).
35. A. Achour, J. B. Ducros, R. L. Porto, M. Boujtita, E. Gautron, L. Le Brizoual, M. A. Djouadi and T. Brousse, *Nano Energy*, **7**, 104 (2014).
36. E. Kao, C. Yang, R. Warren, A. Kozinda and L. Lin, *Sens. Actuators A Phys.*, **240**, 160 (2016).
37. Y. Haldorai, D. Arreaga-Salas, C. S. Rak, Y. S. Huh, Y.-K. Han and W. Voit, *Electrochim. Acta*, **220**, 465 (2016).
38. Y. Xie and X. Fang, *Electrochim. Acta*, **120**, 273 (2014).

39. Y. Xie and R. Gao, *J. Alloys Compd.*, **725**, 1 (2017).
40. H. Yi, X. Chen, H. Wang and X. Wang, *Electrochim. Acta*, **116**, 372 (2014).
41. C. Shang, S. Dong, S. Wang, D. Xiao, P. Han, X. Wang, L. Gu and G. Cui, *ACS Nano*, **7**, 5430 (2013).
42. X. Lu, T. Liu, T. Zhai, G. Wang, M. Yu, S. Xie, Y. Ling, C. Liang, Y. Tong and Y. Li, *Adv. Energy Mater.*, **4**, 1300994 (2014).
43. X. Peng, K. Huo, J. Fu, X. Zhang, B. Gao and P. K. Chu, *Chem. Comm.*, **49**, 10172 (2013).
44. C. Xia, Y. Xie, W. Wang and H. Du, *Synth. Met.*, **192**, 93 (2014).
45. H. Du, Y. Xie, C. Xia, W. Wang and F. Tian, *New J. Chem.*, **38**, 1284 (2014).
46. Y. Xie, C. Xia, H. Du and W. Wang, *J. Power Sources*, **286**, 561 (2015).
47. Y. Xie and D. Wang, *J. Alloys Compd.*, **665**, 323 (2016).
48. L. Lu and Y. Xie, *New J. Chem.*, **41**, 335 (2017).
49. C. Xia, Y. Xie, H. Du and W. Wang, *J. Nanopart. Res.*, **17**, 30 (2015).
50. Y. Xie and F. Tian, *Mater. Sci. Eng. B*, **215**, 64 (2017).
51. P. Lu, E. Halvorsen, P. Ohlckers, L. Müller, S. Leopold, M. Hoffmann, K. Grigoras, J. Ahopelto, M. Prunnila and X. Chen, *Electrochim. Acta*, **248**, 397 (2017).
52. Y. Liu, R. Xiao, Y. Qiu, Y. Fang and P. Zhang, *Electrochim. Acta*, **213**, 393 (2016).
53. C. Zhu, P. Yang, D. Chao, X. Wang, X. Zhang, S. Chen, B. K. Tay, H. Huang, H. Zhang and W. Mai, *Adv. Mater.*, **27**, 4566 (2015).
54. D. Shu, C. Lv, F. Cheng, C. He, K. Yang, J. Nan and L. Long, *Int. J. Electrochem. Sci.*, **8**, 1209 (2013).
55. D. Choi and P. N. Kumta, *Electrochem. Solid-State Lett.*, **8**, A418 (2005).
56. R. Lucio-Porto, S. Bouhtiyya, J. F. Pierson, A. Morel, F. Capon, P. Boulet and T. Brousse, *Electrochim. Acta*, **141**, 203 (2014).
57. J. Zhao, B. Liu, S. Xu, J. Yang and Y. Lu, *J. Alloys Compd.*, **651**, 785 (2015).
58. X. Lu, M. Yu, T. Zhai, G. Wang, S. Xie, T. Liu, C. Liang, Y. Tong and Y. Li, *Nano Lett.*, **13**, 2628 (2013).
59. A. M. Glushenkov, D. Hulicova-Jurcakova, D. Llewellyn, G. Q. Lu and Y. Chen, *Chem. Mater.*, **22**, 914 (2010).
60. H.-M. Lee, G. H. Jeong, S.-W. Kim and C.-K. Kim, *Appl. Surf. Sci.*, **400**, 194 (2017).
61. Y. Wu and F. Ran, *J. Power Sources*, **344**, 1 (2017).
62. G.-H. An, D.-Y. Lee and H.-J. Ahn, *J. Mater. Chem. A*, **5**, 19714 (2017).
63. B. Gao, X. Li, X. Guo, X. Zhang, X. Peng, L. Wang, J. Fu, P. K. Chu and K. Huo, *Adv. Mater. Interfaces*, **2**, 1500211 (2015).
64. N. Ouldhamadouche, A. Achour, R. Lucio-Porto, M. Islam, S. Solaymani, A. Arman, A. Ahmadpourian, H. Achour, L. Le Brizoual, M. A. Djouadi and T. Brousse, *J. Mater. Sci. Technol.*, **34**, 976 (2018).
65. Y. Liu, L. Liu, Y. Tan, L. Niu, L. Kong, L. Kang and F. Ran, *Electrochim. Acta*, **262**, 66 (2018).
66. J. Balamurugan, G. Karthikeyan, T. D. Thanh, N. H. Kim and J. H. Lee, *J. Power Sources*, **308**, 149 (2016).
67. R. Wang, J. Lang, P. Zhang, Z. Lin and X. Yan, *Adv. Fun. Mater.*, **25**, 2270 (2015).
68. E. Eustache, R. Frappier, R. L. Porto, S. Bouhtiyya, J.-F. Pierson and T. Brousse, *Electrochem. Commun.*, **28**, 104 (2013).
69. R. Wang, X. Yan, J. Lang, Z. Zheng and P. Zhang, *J. Mater. Chem. A*, **2**, 12724 (2014).
70. Y. Yang, L. Zhao, K. Shen, Y. Liu, X. Zhao, Y. Wu, Y. Wang and F. Ran, *J. Power Sources*, **333**, 61 (2016).
71. Y. Su and I. Zhitomirsky, *J. Power Sources*, **267**, 235 (2014).
72. Y. Xu, J. Wang, B. Ding, L. Shen, H. Dou and X. Zhang, *ChemElectroChem.*, **2**, 2020 (2015).
73. A. Achour, R. Lucio-Porto, M. Chaker, A. Arman, A. Ahmadpourian, M. A. Soussou, M. Boujtita, L. Le Brizoual, M. A. Djouadi and T. Brousse, *Electrochem. Commun.*, **77**, 40 (2017).
74. Y. Ruan, L. Lv, Z. Li, C. Wang and J. Jiang, *Nanoscale.*, **9**, 18032 (2017).
75. H. Cui, G. Zhu, X. Liu, F. Liu, Y. Xie, C. Yang, T. Lin, H. Gu and F. Huang, *Adv. Sci.*, **2**, 1500126 (2015).
76. B. Das, M. Behm, G. Lindbergh, M. V. Reddy and B. V. R. Chowdari, *Adv. Powder Technol.*, **26**, 783 (2015).
77. A. Śliwak, A. Moyseowicz and G. Gryglewicz, *J. Mater. Chem. A*, **5**, 5680 (2017).
78. L. Xu, L. Sun, J. Feng, L. Qi, I. Muhammad, J. Maher, X. Cheng and W. Song, *RSC Adv.*, **7**, 44619 (2017).
79. S. Wang, C. Sun, Y. Shao, Y. Wu, L. Zhang and X. Hao, *Small.*, **13**, 1603330 (2017).
80. S. Bouhtiyya, R. Lucio Porto, B. Laïk, P. Boulet, F. Capon, J. P. Pereira-Ramos, T. Brousse and J. F. Pierson, *Scripta Mater.*, **68**, 659 (2013).
81. W.-B. Zhang, X.-J. Ma, A. Loh, X. Li, F. C. Walsh and L.-B. Kong, *ACS Energy Lett.*, **2**, 336 (2017).
82. M.-S. Balogun, Y. Zeng, W. Qiu, Y. Luo, A. Onasanya, T. K. Olaniyi and Y. Tong, *J. Mater. Chem. A*, **4**, 9844 (2016).
83. Y. Yu, W. Gao, Z. Shen, Q. Zheng, H. Wu, X. Wang, W. Song and K. Ding, *J. Mater. Chem. A*, **3**, 16633 (2015).
84. A. R. Ko, S.-B. Han, Y.-W. Lee and K.-W. Park, *Phys. Chem. Chem. Phys.*, **13**, 12705 (2011).
85. D. Ruan, R. Lin, K. Jiang, X. Yu, Y. Zhu, Y. Fu, Z. Wang, H. Yan and W. Mai, *ACS Appl. Mater. Interfaces*, **9**, 29699 (2017).
86. Y. Yang, R. Kirchgeorg, R. Hahn and P. Schmuki, *Electrochem. Commun.*, **43**, 31 (2014).
87. O. Kartachova, A. M. Glushenkov, Y. Chen, H. Zhang, X. J. Dai and Y. Chen, *J. Power Sources*, **220**, 298 (2012).
88. E. J. Lee, L. Lee, M. A. Abbas and J. H. Bang, *Phys. Chem. Chem. Phys.*, **19**, 21140 (2017).
89. O. Kartachova, A. M. Glushenkov, Y. Chen, H. Zhang and Y. Chen, *J. Mater. Chem. A*, **1**, 7889 (2013).
90. M. Yu, X. Cheng, Y. Zeng, Z. Wang, Y. Tong, X. Lu and S. Yang, *Ang. Chem. Int. Ed.*, **55**, 6762 (2016).
91. Y.-J. B. Ting, K. Lian and N. Kherani, *ECS Trans.*, **35**, 133 (2011).
92. S. I. U. Shah, A. L. Hector and J. R. Owen, *J. Power Sources*, **266**, 456 (2014).
93. G. Ma, Z. Wang, B. Gao, T. Ding, Q. Zhong, X. Peng, J. Su, B. Hu, L. Yuan, P. K. Chu, J. Zhou and K. Huo, *J. Mater. Chem. A*, **3**, 14617 (2015).
94. L. Chen, C. Liu and Z. Zhang, *Electrochim. Acta*, **245**, 237 (2017).
95. P. Pande, A. Deb, A. E. S. Sleightholme, A. Djire, P. G. Rasmussen, J. Penner-Hahn and L. T. Thompson, *J. Power Sources*, **289**, 154 (2015).

96. C. Chen, D. Zhao and X. Wang, *Mater. Chem. Phy.*, **97**, 156 (2006).
97. R. A. Janes, M. Aldissi and R. B. Kaner, *Chem. Mater.*, **15**, 4431 (2003).
98. X. Lu, G. Wang, T. Zhai, M. Yu, S. Xie, Y. Ling, C. Liang, Y. Tong and Y. Li, *Nano Lett.*, **12**, 5376 (2012).
99. B. Avasarala and P. Haldar, *Electrochim. Acta*, **55**, 9024 (2010).
100. K. Grigoras, J. Keskinen, L. Grönberg, E. Yli-Rantala, S. Laakso, H. Välimäki, P. Kauranen, J. Ahopelto and M. Prunnila, *Nano Energy*, **26**, 340 (2016).
101. A. Achour, M. Chaker, H. Achour, A. Arman, M. Islam, M. Mardani, M. Boujtita, L. Le Brizoual, M. A. Djouadi and T. Brousse, *J. Power Sources*, **359**, 349 (2017).
102. B. M. Gray, A. L. Hector, M. Jura, J. R. Owen and J. Whittam, *J. Mater. Chem. A*, **5**, 4550 (2017).
103. A. Djire, J. Y. Ishimwe, S. Choi and L. T. Thompson, *Electrochem. Commun.*, **77**, 19 (2017).
104. A. Morel, Y. Borjon-Piron, R. L. Porto, T. Brousse and D. Bélanger, *J. Electrochem. Soc.*, **163**, A1077 (2016).
105. D. Choi, G. E. Blomgren and P. N. Kumta, *Adv. Mater.*, **18**, 1178 (2006).
106. P. J. Hanumantha, M. K. Datta, K. Kadakia, C. Okoli, P. Patel and P. N. Kumta, *Electrochim. Acta*, **207**, 37 (2016).
107. P. J. Hanumantha, M. K. Datta, K. S. Kadakia, D. H. Hong, S. J. Chung, M. C. Tam, J. A. Poston, A. Manivannan and P. N. Kumta, *J. Electrochem. Soc.*, **160**, A2195 (2013).
108. O. Bondarchuk, A. Morel, D. Bélanger, E. Goikolea, T. Brousse and R. Mysyk, *J. Power Sources*, **324**, 439 (2016).
109. B. Wang, Z. Chen, G. Lu, T. Wang and Y. Ge, *Mater. Res. Bull.*, **76**, 37 (2016).
110. C. M. Ghimbeu, E. Raymundo-Piñero, P. Fioux, F. Béguin and C. Vix-Guterl, *J. Mater. Chem.*, **21**, 13268 (2011).
111. N. Fechler, G. A. Tiruye, R. Marcilla and M. Antonietti, *RSC Adv.*, **4**, 26981 (2014).
112. D. Choi, P. H. Jampani, J. R. P. Jayakody, S. G. Greenbaum and P. N. Kumta, *Mater. Sci. Eng. B*, **230**, 8 (2018).
113. X. Zhou, H. Chen, D. Shu, C. He and J. Nan, *J. Phys. Chem. Solids.*, **70**, 495 (2009).
114. S. Ghosh, T. Mathews, B. Gupta, A. Das, N. G. Krishna and M. Kamruddin, *Nano-Struct. Nano-Objects*, **10**, 42 (2017).
115. H.-h. Liu, H.-l. Zhang, H.-b. Xu, T.-p. Lou, Z.-t. Sui and Y. Zhang, *J. Electrochem. Soc.*, **165**, A97 (2018).
116. X. Xiao, X. Peng, H. Jin, T. Li, C. Zhang, B. Gao, B. Hu, K. Huo and J. Zhou, *Adv. Mater.*, **25**, 5091 (2013).
117. P. Wang, R. Wang, J. Lang, X. Zhang, Z. Chen and X. Yan, *J. Mater. Chem. A*, **4**, 9760 (2016).
118. D. Choi and P. N. Kumta, *J. Amer. Ceram. Soc.*, **94**, 2371 (2011).
119. M. Liu, L. Zhang, P. Han, X. Han, H. Du, X. Yue, Z. Zhang, H. Zhang and G. Cui, *Part. Part. Syst. Char.*, **32**, 1006 (2015).
120. Y. Wang, M. Jiang, Y. Yang and F. Ran, *Electrochim. Acta*, **222**, 1914 (2016).
121. L. Jiang, L. Lin, F. Yan, B. Fan, Y. Chen and Y. Qiu, *Ceram. Int.*, **43**, 9226 (2017).
122. R. L. Porto, R. Frappier, J. B. Ducros, C. Aucher, H. Mosqueda, S. Chenu, B. Chavillon, F. Tessier, F. Cheviré and T. Brousse, *Electrochim. Acta*, **82**, 257 (2012).
123. Q. Zheng, A. Kvit, Z. Cai, Z. Ma and S. Gong, *J. Mater. Chem. A*, **5**, 12528 (2017).
124. D. Shu, H. Cheng, C. Lv, M. A. Asi, L. Long, C. He, X. Zou and Z. Kang, *Int. J. Hydrog. Energy*, **39**, 16139 (2014).
125. M. Yu, Y. Han, X. Cheng, L. Hu, Y. Zeng, M. Chen, F. Cheng, X. Lu and Y. Tong, *Adv. Mater.*, **27**, 3085 (2015).
126. O. Kartachova, Y. Chen, R. Jones, Y. Chen, H. Zhang and A. M. Glushenkov, *J. Mater. Chem. A*, **2**, 12940 (2014).
127. H. Tomiyasu, H. Shikata, K. Takao, N. Asanuma, S. Taruta and Y.-Y. Park, *Sc. Rep.*, **7**, 45048 (2017).
128. N. Choudhary, C. Li, J. Moore, N. Nagaiah, L. Zhai, Y. Jung and J. Thomas, *Adv. Mater.*, **29**, 1605336 (2017).
129. M. Rajkumar, C.-T. Hsu, T.-H. Wu, M.-G. Chen and C.-C. Hu, *Progress in Natural Science: Mater. Int.*, **25**, 527 (2015).
130. A. Djire, O. T. Ajenifujah, A. E. S. Sleightholme, P. Rasmussen and L. T. Thompson, *J. Power Sources*, **275**, 159 (2015).
131. M. Inagaki, H. Konno and O. Tanaike, *J. Power Sources*, **195**, 7880 (2010).
132. S. Ghosh, S. R. Polaki, M. Kamruddin, S. M. Jeong and K. K. Ostrikov, *J. Phys. D: Appl. Phys.*, **51**, 145303 (2018).
133. Q. Wang, J. Yan and Z. Fan, *Energy Environ. Sci.*, **9**, 729 (2016).
134. B. Mendoza-Sánchez and Y. Gogotsi, *Adv. Mater.*, **28**, 6104 (2016).
135. J. M. Soon and K. P. Loh, *Electrochem. Solid-State Lett.*, **10**, A250 (2007).
136. K. S. Kumar, N. Choudhary, Y. Jung and J. Thomas, *ACS Energy Lett.*, **3**, 482 (2018).
137. M. A. Bissett, S. D. Worrall, I. A. Kinloch and R. A. W. Dryfe, *Electrochim. Acta*, **201**, 30 (2016).
138. R. K. Mishra, S. Manivannan, K. Kim, H.-I. Kwon and S.H. Jin, *Curr. Appl. Phys.*, **18**, 345 (2018).
139. I. Shown, A. Ganguly, L. C. Chen and K. H. Chen, *Energy Sci. Eng.*, **3**, 2 (2015).
140. M. Huang, F. Li, F. Dong, Y. X. Zhang and L. L. Zhang, *J. Mater. Chem. A*, **3**, 21380 (2015).
141. J. Yan, Q. Wang, T. Wei and Z. Fan, *Adv. Energy Mater.*, **4**, 1300816 (2014).
142. S. S. Karade, D. P. Dubal and B. R. Sankapal, *RSC Adv.*, **6**, 39159 (2016).
143. A. Hossain, P. Bandyopadhyay, P. S. Guin and S. Roy, *Appl. Mater. Today*, **9**, 300 (2017).
144. M. Acerce, D. Voiry and M. Chhowalla, *Nat. Nanotechnol.*, **10**, 313 (2015).

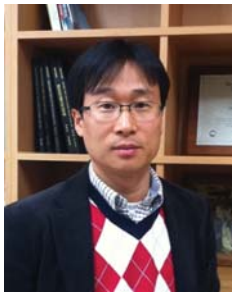

Sang Mun Jeong is a professor in Department of Chemical Engineering, Chungbuk National University and a director of the Korean Institute of Chemical Engineers. He obtained his Ph.D. degree in Chemical Engineering from Korea Advanced Institute of Science and Technology (KAIST) in 1999. He worked previously at CPE Lyon (France), University of Nottingham (UK), University of Utah (US), LG Chemical and Korea Atomic Energy Research Institute (KAERI). He has published over 90 articles on chemical and electrochemical reactions for application to energy, environment and materials and is cited as the inventor on over 20 patents.